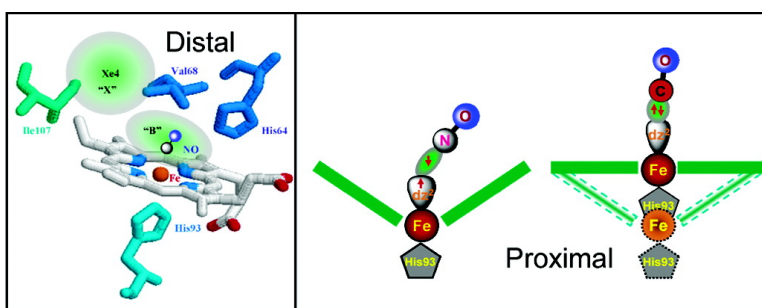


## Temperature-Dependent Studies of NO Recombination to Heme and Heme Proteins

Dan Ionascu, Flaviu Gruia, Xiong Ye, Anchi Yu, Florin Rosca, Chris Beck, Andrey Demidov, John S. Olson, and Paul M. Champion

*J. Am. Chem. Soc.*, **2005**, 127 (48), 16921-16934 • DOI: 10.1021/ja054249y • Publication Date (Web): 10 November 2005

Downloaded from <http://pubs.acs.org> on March 25, 2009



### More About This Article

Additional resources and features associated with this article are available within the HTML version:

- Supporting Information
- Links to the 10 articles that cite this article, as of the time of this article download
- Access to high resolution figures
- Links to articles and content related to this article
- Copyright permission to reproduce figures and/or text from this article

[View the Full Text HTML](#)

## Temperature-Dependent Studies of NO Recombination to Heme and Heme Proteins

Dan Ionascu,<sup>†</sup> Flaviu Gruia,<sup>†</sup> Xiong Ye,<sup>†</sup> Anchi Yu,<sup>†</sup> Florin Rosca,<sup>†</sup> Chris Beck,<sup>†</sup> Andrey Demidov,<sup>†</sup> John S. Olson,<sup>‡</sup> and Paul M. Champion\*<sup>†</sup>

Contribution from the Department of Physics and Center for Interdisciplinary Research on Complex Systems, Northeastern University, Boston, Massachusetts 02115, and the Department of Biochemistry and Cell Biology and the W. M. Keck Center for Computational Biology, Rice University, Houston, Texas 77005

Received June 28, 2005; E-mail: p.champion@neu.edu

**Abstract:** The rebinding kinetics of NO to the heme iron of myoglobin (Mb) is investigated as a function of temperature. Below 200 K, the transition-state enthalpy barrier associated with the fastest (~10 ps) recombination phase is found to be zero and a slower geminate phase (~200 ps) reveals a small enthalpic barrier (~3 ± 1 kJ/mol). Both of the kinetic rates slow slightly in the myoglobin (Mb) samples above 200 K, suggesting that a small amount of protein relaxation takes place above the solvent glass transition. When the temperature dependence of the NO recombination in Mb is studied under conditions where the distal pocket is mutated (e.g., V68W), the rebinding kinetics lack the slow phase. This is consistent with a mechanism where the slower (~200 ps) kinetic phase involves transitions of the NO ligand into the distal heme pocket from a more distant site (e.g., in or near the Xe4 cavity). Comparison of the temperature-dependent NO rebinding kinetics of native Mb with that of the bare heme (PPIX) in glycerol reveals that the fast (enthalpically barrierless) NO rebinding process observed below 200 K is independent of the presence or absence of the proximal histidine ligand. In contrast, the slowing of the kinetic rates above 200 K in MbNO disappears in the absence of the protein. Generally, the data indicate that, in contrast to CO, the NO ligand binds to the heme iron through a "harpoon" mechanism where the heme iron out-of-plane conformation presents a negligible enthalpic barrier to NO rebinding. These observations strongly support a previous analysis (Srajer et al. *J. Am. Chem. Soc.* **1988**, *110*, 6656–6670) that primarily attributes the low-temperature stretched exponential rebinding of MbCO to a quenched distribution of heme geometries. A simple model, consistent with this prior analysis, is presented that explains a variety of MbNO rebinding experiments, including the dependence of the kinetic amplitudes on the pump photon energy.

### Introduction

Myoglobin (Mb) is a small globular heme protein that stores oxygen reversibly in muscle tissue. In addition to O<sub>2</sub>, Mb also binds CO and NO, two other diatomic ligands that are involved in a variety of cellular signaling processes when they interact with specific heme proteins.<sup>1–14</sup> Because these ligands are all

photolabile to varying degrees,<sup>15</sup> Mb has been used as a convenient sample for studies of the dynamics of diatomic ligand binding to the heme and the associated protein response. Over the years, Mb has become one of the most intensely studied heme proteins and a wide variety of physical methods<sup>16–52</sup> have been applied to elucidate its equilibrium, photophysical, and

<sup>†</sup> Northeastern University.

<sup>‡</sup> Rice University.

- (1) Moncada, S.; Palmer, R. M. J.; Higgs, E. A. *Pharmacol. Rev.* **1991**, *43*, 109–142.
- (2) Marletta, M. A. *J. Biol. Chem.* **1993**, *268*, 12231–12234.
- (3) Dawson, T. M.; Dawson, V. L.; Snyder, S. H. *Molecular Mechanisms of Nitric-Oxide Actions in the Brain*, 1994; pp 76–85.
- (4) Dawson, T. M.; Snyder, S. H. *J. Neurosci.* **1994**, *14*, 5147–5159.
- (5) Moncada, S. *J. Hypertens.* **1994**, *12*, S35–S39.
- (6) Nelson, R. J.; Demas, G. E.; Huang, P. L.; Fishman, M. C.; Dawson, V. L.; Dawson, T. M.; Snyder, S. H. *Nature* **1995**, *378*, 383–386.
- (7) Shelver, D.; Kerby, R. L.; He, Y.; Roberts, G. P. *Proc. Natl. Acad. Sci. U.S.A.* **1997**, *94*, 11216–11220.
- (8) Gow, A. J.; Stamler, J. S. *Nature* **1998**, *391*, 169–173.
- (9) Zhao, Y.; Brandish, P. E.; Ballou, D. P.; Marletta, M. A. *Proc. Natl. Acad. Sci. U.S.A.* **1999**, *96*, 14753–14758.
- (10) Ignarro, L. J.; Cirino, G.; Casini, A.; Napoli, C. *J. Cardiovasc. Pharmacol.* **1999**, *34*, 879–886.
- (11) Wardrop, S. L.; Watts, R. N.; Richardson, D. R. *Biochemistry* **2000**, *39*, 2748–2758.
- (12) Kumazaki, S.; Nakajima, H.; Sakaguchi, T.; Nakagawa, E.; Shinohara, H.; Yoshihara, K.; Aono, S. *J. Biol. Chem.* **2000**, *275*, 38378–38383.

- (13) Uchida, T.; Ishikawa, H.; Ishimori, K.; Morishima, I.; Nakajima, H.; Aono, S.; Mizutani, Y.; Kitagawa, T. *Biochemistry* **2000**, *39*, 12747–12752.
- (14) Fogel, U.; Merx, M. W.; Godecke, A.; Decking, U. K. M.; Schrader, J. *Proc. Natl. Acad. Sci. U.S.A.* **2001**, *98*, 735–740.
- (15) Ye, X.; Demidov, A. A.; Champion, P. M. *J. Am. Chem. Soc.* **2002**, *124*, 5914–5924.
- (16) Perutz, M. F. *Nature* **1970**, *228*, 726–739.
- (17) Tamura, M.; Asakura, T.; Yonetani, T. *Biochim. Biophys. Acta* **1973**, *295*, 467–479.
- (18) Austin, R. H.; Beeson, K. W.; Eisenstein, L.; Frauenfelder, H.; Gunsalus, I. C. *Biochemistry* **1975**, *14*, 5355–5373.
- (19) Spertalian, K.; Lang, G.; Yonetani, T. *Biochim. Biophys. Acta* **1976**, *428*, 281–290.
- (20) Uyeda, M.; Peisach, J. *Biochemistry* **1981**, *20*, 2028–2035.
- (21) Caughey, W. S.; Shimada, H.; Choc, M. G.; Tucker, M. P. *Proc. Natl. Acad. Sci. U.S.A.* **1981**, *78*, 2903–2907.
- (22) Lamar, G. N.; Deropp, J. S.; Latosgrzynski, L.; Balch, A. L.; Johnson, R. B.; Smith, K. M.; Parish, D. W.; Cheng, R. J. *J. Am. Chem. Soc.* **1983**, *105*, 782–787.
- (23) Ansari, A.; Berendzen, J.; Braunstein, D.; Cowen, B. R.; Frauenfelder, H.; Hong, M. K.; Iben, I. E. T.; Johnson, J. B.; Ormos, P.; Sauke, T. B.; Scholl, R.; Schulte, A.; Steinbach, P. J.; Vittitow, J.; Young, R. D. *Biophys. Chem.* **1987**, *26*, 337–355.

dynamic properties. As such, Mb has become a genuine prototype for the study of heme proteins. Surprisingly, even with the extensive studies performed on such an apparently simple system, there are still a variety of unanswered questions surrounding the process of diatomic ligand binding.

Kinetic studies of heme systems usually involve ligand photodissociation, where a photon is absorbed by the heme group and the bond between the iron and the diatomic ligand is broken. Following this process, the diatomic ligand can either return and rebind to the heme (a geminate process) or it can escape to the immediate protein environment (cavities in the protein matrix), pass through fluctuating entry and exit channels, and ultimately pass out of the protein and into the solvent.

The rebinding of the NO molecule to myoglobin provides an excellent test case for the study of the final binding step(s) involving bond formation at the heme. This is because the geminate rebinding is fast (picosecond time scale) and nearly (>95%) complete. In contrast, the other diatomics (especially CO) have much smaller geminate amplitudes so that their kinetics are dominated by the ligand escape and re-entry processes. Moreover, the interaction of the NO molecule with heme systems is an important reaction to study because many physiological effects and biological functions of NO have been discovered (neurotransmission,<sup>1,3,4,53</sup> regulation of vasodilatation,<sup>5,10,53–56</sup> platelet aggregation,<sup>57</sup> and immune response<sup>58,59</sup>).

Because of the ultrafast (picosecond) nature of the NO rebinding process, and the experimental difficulties associated with temperature-dependent studies on such short time scales, there are no reports of any direct experimental determination of the recombination barrier for NO binding to Mb. On the other hand, studies of heme model compounds<sup>60–64</sup> as well as indirect studies<sup>28,38,45,65–67</sup> have suggested that the recombination barrier for NO is indeed very small compared with that of CO and O<sub>2</sub>.

Because of the relatively slow nature of the CO rebinding process and the stability of the CO adduct, the CO recombination to the heme has been historically the most well-studied heme kinetic process.<sup>18</sup> For example, it has been determined<sup>68,69</sup> that the CO geminate recombination has a weakly nonexponential behavior above 260 K that arises from distal pocket protein relaxation on the same time scale (10–100 ns) as that for ligand escape. However, below 200 K, the recombination kinetics deviates much more dramatically from a simple exponential response. The pioneering experiments performed by Frauenfelder and co-workers<sup>18,33</sup> have determined that below 200 K the molecular ensemble is kinetically heterogeneous because of trapped protein conformational substates that bind the CO molecule with different rates. The distribution of protein molecules “frozen” in different conformational states gives rise to an asymmetric distribution of rebinding barriers<sup>18,24</sup> (in the range 5–15 kJ/mol) and highly stretched nonexponential rebinding kinetics.

We have proposed that one of the key conformational coordinates giving rise to this type of rebinding distribution in heme systems involves the protein induced heme geometry, which can be conveniently (if simplistically) quantified by two moments, the mean iron out-of-heme-plane displacement and its protein induced mean square disorder.<sup>24,70,71</sup> The nonexponential rebinding behavior appears at low temperatures because the rebinding of the CO molecule to the heme iron occurs on a time scale faster than the interconversion between the protein conformational substates, making the ensemble inhomogeneous with respect to the kinetics measurement. On the other hand, at

- (24) Srajer, V.; Reinisch, L.; Champion, P. M. *J. Am. Chem. Soc.* **1988**, *110*, 6656–6670.
- (25) Petrich, J. W.; Martin, J. L. *Chem. Phys.* **1989**, *131*, 31–47.
- (26) Magliozzo, R. S.; Peisach, J. *Biochemistry* **1993**, *32*, 8446–8456.
- (27) Egeberg, K. D.; Springer, B. A.; Sligar, S. G.; Carver, T. E.; Rohlfs, R. J.; Olson, J. S. *J. Biol. Chem.* **1990**, *265*, 11788–11795.
- (28) Carver, T. E.; Rohlfs, R. J.; Olson, J. S.; Gibson, Q. H.; Blackmore, R. S.; Springer, B. A.; Sligar, S. G. *J. Biol. Chem.* **1990**, *265*, 20007–20020.
- (29) Young, R. D.; Frauenfelder, H.; Johnson, J. B.; Lamb, D. C.; Nienhaus, G. U.; Philipp, R.; Scholl, R. *Chem. Phys.* **1991**, *158*, 315–327.
- (30) Petrich, J. W.; Lambry, J. C.; Kuczera, K.; Karplus, M.; Poyart, C.; Martin, J. L. *Biochemistry* **1991**, *30*, 3975–3987.
- (31) Genberg, L.; Richard, L.; Mclendon, G.; Miller, R. J. D. *Science* **1991**, *251*, 1051–1054.
- (32) Miller, R. J. D. *Annu. Rev. Phys. Chem.* **1991**, *42*, 581–614.
- (33) Steinbach, P. J.; Ansari, A.; Berendzen, J.; Braunstein, D.; Chu, K.; Cowen, B. R.; Ehrenstein, D.; Frauenfelder, H.; Johnson, J. B.; Lamb, D. C.; Luck, S.; Mourant, J. R.; Nienhaus, G. U.; Ormos, P.; Philipp, R.; Xie, A. H.; Young, R. D. *Biochemistry* **1991**, *30*, 3988–4001.
- (34) Frauenfelder, H.; Sligar, S. G.; Wolynes, P. G. *Science* **1991**, *254*, 1598–1603.
- (35) Nienhaus, G. U.; Frauenfelder, H.; Parak, F. *Phys. Rev. B: Condens. Matter* **1991**, *43*, 3345–3350.
- (36) Quillin, M. L.; Arduini, R. M.; Olson, J. S.; Phillips, G. N., Jr. *J. Mol. Biol.* **1993**, *234*, 140–155.
- (37) Lim, M.; Jackson, T. A.; Anfinsen, P. A. *Proc. Natl. Acad. Sci. U.S.A.* **1993**, *90*, 8302.
- (38) Ikeda-Saito, M.; Dou, Y.; Yonetani, T.; Olson, J. S.; Li, T. S.; Regan, R.; Gibson, Q. H. *J. Biol. Chem.* **1993**, *268*, 6855–6857.
- (39) Li, H. Y.; Elber, R.; Straub, J. E. *J. Biol. Chem.* **1993**, *268*, 17908–17916.
- (40) Sage, J. T.; Ivanov, D.; Keim, M.; Powell, J. R.; Asher, S. A.; Champion, P. M. *Biophys. J.* **1994**, *66A*, 271.
- (41) Zhu, L. Y.; Sage, J. T.; Champion, P. M. *Science* **1994**, *266*, 629–632.
- (42) Deak, J.; Richard, L.; Pereira, M.; Chui, H. L.; Miller, R. J. D. *Methods Enzymol.* **1994**, *232*, 322–360.
- (43) Springer, B. A.; Sligar, S. G.; Olson, J. S.; Phillips, G. N., Jr. *Chem. Rev.* **1994**, *94*, 699–714.
- (44) Carlson, M. L.; Regan, R.; Elber, R.; Li, H. Y.; Phillips, G. N.; Olson, J. S.; Gibson, Q. H. *Biochemistry* **1994**, *33*, 10597–10606.
- (45) Olson, J. S.; Phillips, G. N., Jr. *J. Biol. Chem.* **1996**, *271*, 17593–17596.
- (46) Sage, J. T.; Champion, P. M. *Comprehensive Supramolecular Chemistry*; Pergamon: Oxford, U.K., 1996; Chapter 6, pp 171–218.
- (47) Sage, J. T.; Jee, W. *J. Mol. Biol.* **1997**, *274*, 21–26.
- (48) Gdoutou, N.; Havlin, R.; Salzman, R.; Debrunner, P. G.; Oldfield, E. *J. Phys. Chem. A* **1998**, *102*, 2342–2350.
- (49) Scott, E. E.; Gibson, Q. H.; Olson, J. S. *J. Biol. Chem.* **2001**, *276*, 5177–5188.
- (50) Nienhaus, K.; Deng, P. C.; Olson, J. S.; Warren, J. J.; Nienhaus, G. U. *J. Biol. Chem.* **2003**, *278*, 42532–42544.
- (51) Sage, J. T. *Encyclopedia of Supramolecular Chemistry*; Marcel Dekker: New York, 2004; pp 636–644.
- (52) Kim, S.; Lim, M. *J. Am. Chem. Soc.* **2005**, *127*, 8908–8909.
- (53) Moncada, S.; Higgs, A. *N. Engl. J. Med.* **1993**, *329*, 2002–2012.

- (54) Kilbourn, R. G.; Gross, S. S.; Jubran, A.; Adams, J.; Griffith, O. W.; Levi, R.; Lodato, R. F. *Proc. Natl. Acad. Sci. U.S.A.* **1990**, *87*, 3629–3632.
- (55) Kilbourn, R. G.; Gross, S. S.; Lodato, R. F.; Adams, J.; Levi, R.; Miller, L. L.; Lachman, L. B.; Griffith, O. W. *J. Natl. Cancer Inst.* **1992**, *84*, 1008–1016.
- (56) Bredt, D. S.; Snyder, S. H. *Annu. Rev. Biochem.* **1994**, *63*, 175–195.
- (57) Pawloski, J. R.; Hess, D. T.; Stamler, J. S. *Nature* **2001**, *409*, 622–626.
- (58) Bani, D.; Masini, E.; Bello, M. G.; Bigazzi, M.; Sacchi, T. B. *Cancer Res.* **1995**, *55*, 5272–5275.
- (59) Fiorucci, S.; Antonelli, E.; Distrutti, E.; Del Soldato, P.; Flower, R. J.; Clark, M. J. P.; Morelli, A.; Perretti, M.; Ignarro, L. J. *Proc. Natl. Acad. Sci. U.S.A.* **2002**, *99*, 15770–15775.
- (60) Miers, J. B.; Postlewaite, J. C.; Zyung, T.; Chen, S.; Roemig, G. R.; Wen, X.; Dlott, D. D.; Szabo, A. J. *Chem. Phys.* **1990**, *93*, 8771–8776.
- (61) Miers, J. B.; Postlewaite, J. C.; Cowen, B. R.; Roemig, G. R.; Lee, I. Y. S.; Dlott, D. D. *J. Chem. Phys.* **1991**, *94*, 1825–1836.
- (62) Traylor, T. G.; Magde, D.; Taube, D. J.; Jongeward, K. A.; Bandyopadhyay, D.; Luo, J. K.; Walda, K. N. *J. Am. Chem. Soc.* **1992**, *114*, 417–429.
- (63) Traylor, T. G.; Magde, D.; Marsters, J.; Jongeward, K.; Wu, G. Z.; Walda, K. J. *Am. Chem. Soc.* **1993**, *115*, 4808–4813.
- (64) Grogan, T. G.; Bag, N.; Traylor, T. G.; Magde, D. *J. Phys. Chem.* **1994**, *98*, 13791–13796.
- (65) Gibson, Q. H.; Olson, J. S.; McKinnin, R. E.; Rohlfs, R. J. *J. Biol. Chem.* **1986**, *261*, 228–239.
- (66) Gibson, Q. H.; Regan, R.; Olson, J. S.; Carver, T. E.; Dixon, B.; Pohajdak, B.; Sharma, P. K.; Vinogradov, S. N. *J. Biol. Chem.* **1993**, *268*, 16993–16998.
- (67) Nutt, D. R.; Meuwly, M. *ChemPhysChem* **2004**, *5*, 1710–1718.
- (68) Lambright, D. G.; Balasubramanian, S.; Boxer, S. G. *Chem. Phys.* **1991**, *158*, 249–260.
- (69) Tian, W. D.; Sage, J. T.; Srajer, V.; Champion, P. M. *Phys. Rev. Lett.* **1992**, *68*, 408–411.
- (70) Srajer, V.; Schomacker, K. T.; Champion, P. M. *Phys. Rev. Lett.* **1986**, *57*, 1267–1270.
- (71) Champion, P. M. *J. Raman Spectrosc.* **1992**, *23*, 557–567.

higher temperatures above 200 K, the interconversion of the protein substates can occur on time scales faster than the CO rebinding process. This leads to kinetic homogeneity within the ensemble and a narrow rate distribution. However, because additional protein relaxation processes also take place at higher temperatures, the free-energy rebinding barrier becomes time dependent and can vary on the same time scale as the kinetics. As a result, nonexponential recombination is also observed near room temperature, even though the source of this nonexponential behavior arises from a homogeneous relaxation process.<sup>69</sup>

The underlying sources of the nonexponential kinetic response in the CO rebinding reactions were determined by using a double pump-pulse kinetic protocol that distinguishes kinetic inhomogeneity from homogeneous relaxation processes<sup>69,72</sup> and allows the time scale for protein conformational interconversion to be determined.<sup>72</sup> As discussed below, we have recently extended this concept to picosecond time scales,<sup>73</sup> using a modified protocol, and have applied it to the MbNO rebinding reaction.

The recombination of the NO molecule to myoglobin is thought to have two geminate phases near room temperature.<sup>30,74–76</sup> Following ultrafast photodissociation<sup>77–81</sup> in the aqueous phase near room temperature, the NO molecule geminately recombines within hundreds of picoseconds, suggesting that it has an effective barrier much smaller than CO, where the recombination rate in aqueous solution is  $\sim 0.35 \times 10^6$  to  $2.5 \times 10^6 \text{ s}^{-1}$  (i.e.,  $\sim 3.0\text{--}0.4 \mu\text{s}$ ) depending on the assumed relaxation function.<sup>69,82,83</sup> Because of the fact that the NO recombination occurs on comparable time scales to the heme/protein relaxation, it has been suggested that the nonexponential MbNO recombination observed near room temperature is due to a time-dependent barrier that develops as the photolyzed heme starts relaxing toward its out-of-plane equilibrium conformation.<sup>30,84</sup> As suggested previously for the CO reaction,<sup>24,85</sup> those conformations that have the highest rebinding barriers are the ones associated with heme conformations where the iron is further out of the heme plane, so the NO binding reaction might be expected to slow as time evolves, giving rise to the nonexponential kinetic response. Studies by Magde and co-workers<sup>86</sup> appear to support this concept by demonstrating that when MbNO loses its proximal histidine at low pH, the nonexponential second phase of the kinetics is eliminated. On the other hand, several kinetic

studies involving cobalt-substituted heme (where the metal does not undergo an out-of-plane displacement<sup>87,88</sup>) reveal little change in the kinetic response and suggest that proximal relaxation is unimportant for the NO binding reaction.<sup>38,75,89</sup> The work presented here indicates that this latter interpretation is correct and that the kinetic changes noted by Duprat et al.<sup>86</sup> involving MbNO at low pH probably arise from a modification of the distal pocket when H64 is protonated and swings out toward the solution.<sup>90–93</sup>

In addition to temperature-dependent kinetic studies, there have also been experiments in which the influence of the protein motion on ligand rebinding is studied as a function of solvent viscosity.<sup>94–96</sup> For example, Shreve and co-workers<sup>96</sup> have carefully studied the effects of glycerol on the amplitudes and rates of the MbNO rebinding reaction at room temperature. Constraints associated with the standard three-state serial kinetics model were noted, and their analysis suggests that a parallel model is needed to explain the kinetics evolution following MbNO photolysis.<sup>96</sup> Analogous constraints on the standard three-state serial model are confirmed by the temperature-dependent NO recombination and site-directed mutant studies reported here. However, we show that if the initial conditions associated with the standard serial model are modified, it can be made consistent with the observations.

The ultrafast kinetics of the MbNO V68 mutants presented here are also consistent with prior studies of MbCO,<sup>27,36,97</sup> where it has been suggested that the size of the aromatic side chains substituted into position 68 can regulate the ligand pathway and rebinding process. There are four known xenon cavities<sup>98</sup> within the myoglobin protein matrix, and these cavities are thought to play an important role in diatomic ligand rebinding and escape by functioning as transient trapping sites.<sup>49,50,67,99–101</sup> The distal valine-68 is adjacent to the heme binding site, and the mutations V68F and V68W introduce large aromatic side chains (phenylalanine and tryptophan, respectively) into the distal pocket,<sup>50,97</sup> completely filling the Xe4 cavity in the case of V68W. It has been shown<sup>49,50,99</sup> that the geminate phases of MbO<sub>2</sub> and MbCO recombination are dramatically increased upon the V68F and V68W mutations, consistent with the fact that the Xe4 cavity becomes inaccessible in the presence of these large amino acids.

- (72) Tian, W. D.; Sage, J. T.; Champion, P. M.; Chien, E.; Sligar, S. G. *Biochemistry* **1996**, *35*, 3487–3502.  
 (73) Yu, A.; Ye, X.; Ionascu, D.; Cao, W.; Champion, P. M. To be submitted, 2005.  
 (74) Cornelius, P. A.; Hochstrasser, R. M.; Steele, A. W. *J. Mol. Biol.* **1983**, *163*, 119–128.  
 (75) Gibson, Q. H.; Regan, R.; Elber, R.; Olson, J. S.; Carver, T. E. *J. Biol. Chem.* **1992**, *267*, 22022–22034.  
 (76) Shreve, A. P.; Franzen, S.; Simpson, M. C.; Woodruff, W. H.; Dyer, R. B. *Biophys. J.* **1997**, *72*, A424.  
 (77) Martin, J. L.; Migus, A.; Poyart, C.; Lecarpentier, Y.; Antonetti, A.; Orszag, A. *Biochem. Biophys. Res. Commun.* **1982**, *107*, 803–810.  
 (78) Anfirrud, P. A.; Han, C.; Hochstrasser, R. M. *Proc. Natl. Acad. Sci. U.S.A.* **1989**, *86*, 8387–8391.  
 (79) Franzen, S.; Bohn, B.; Poyart, C.; Martin, J. L. *Biochemistry* **1995**, *34*, 1224–1237.  
 (80) Rosca, F.; Kumar, A. T. N.; Ionascu, D.; Sjodin, T.; Demidov, A. A.; Champion, P. M. *J. Chem. Phys.* **2001**, *114*, 10884–10898.  
 (81) Champion, P. M.; Rosca, F.; Ionascu, D.; Cao, W. X.; Ye, X. *Faraday Discuss.* **2004**, *127*, 123–135.  
 (82) Henry, E. R.; Sommer, J. H.; Hofrichter, J.; Eaton, W. A. *J. Mol. Biol.* **1983**, *166*, 443–451.  
 (83) Lambright, D. G.; Balasubramanian, S.; Decatur, S. M.; Boxer, S. G. *Biochemistry* **1994**, *33*, 5518–5525.  
 (84) Meuwly, M.; Becker, O. M.; Stote, R.; Karplus, M. *Biophys. Chem.* **2002**, *98*, 183–207.  
 (85) Srajer, V.; Champion, P. M. *Biochemistry* **1991**, *30*, 7390–7402.  
 (86) Duprat, A. F.; Traylor, T. G.; Wu, G. Z.; Coletta, M.; Sharma, V. S.; Walda, K. N.; Magde, D. *Biochemistry* **1995**, *34*, 2634–2644.

- (87) Hoard, J. L.; Scheidt, W. R. *Proc. Natl. Acad. Sci. U.S.A.* **1973**, *70*, 3919–3922.  
 (88) Fermi, G.; Perutz, M. F.; Dickinson, L. C.; Chien, J. C. W. *J. Mol. Biol.* **1982**, *155*, 495–505.  
 (89) Kholodenko, Y.; Gooding, E. A.; Dou, Y.; Ikeda-Saito, M.; Hochstrasser, R. M. *Biochemistry* **1999**, *38*, 5918–5924.  
 (90) Morikis, D.; Champion, P. M.; Springer, B. A.; Sligar, S. G. *Biochemistry* **1989**, *28*, 4791–4800.  
 (91) Sage, J. T.; Morikis, D.; Champion, P. M. *Biochemistry* **1991**, *30*, 1227–1237.  
 (92) Sage, J. T.; Morikis, D.; Li, P. S.; Champion, P. M. *Biophys. J.* **1992**, *61*, 1041–1044.  
 (93) Yang, F.; Phillips, G. N., Jr. *J. Mol. Biol.* **1996**, *256*, 762–774.  
 (94) Ansari, A.; Jones, C. M.; Henry, E. R.; Hofrichter, J.; Eaton, W. A. *Science* **1992**, *256*, 1796–1798.  
 (95) Kleiwert, T.; Doster, W.; Leyser, H.; Petry, W.; Schwarz, V.; Settles, M. *Biochemistry* **1998**, *37*, 717–733.  
 (96) Shreve, A. P.; Franzen, S.; Simpson, M. C.; Dyer, R. B. *J. Phys. Chem. B* **1999**, *103*, 7969–7975.  
 (97) Quillin, M. L.; Li, T. S.; Olson, J. S.; Phillips, G. N.; Dou, Y.; Ikeda-Saito, M.; Regan, R.; Carlson, M.; Gibson, Q. H.; Li, H. Y.; Elber, R. *J. Mol. Biol.* **1995**, *245*, 416–436.  
 (98) Tilton, R. F., Jr.; Kuntz, I. D., Jr.; Petsko, G. A. *Biochemistry* **1984**, *23*, 2849–2857.  
 (99) Dantsker, D.; Samuni, U.; Friedman, A. J.; Yang, M.; Ray, A.; Friedman, J. M. *J. Mol. Biol.* **2002**, *315*, 239–251.  
 (100) Lamb, D. C.; Nienhaus, K.; Arcovito, A.; Draghi, F.; Miele, A. E.; Brunori, M.; Nienhaus, G. U. *J. Biol. Chem.* **2002**, *277*, 11636–11644.  
 (101) Tetreau, C.; Blouquit, Y.; Novikov, E.; Quiniou, E.; Lavalette, D. *Biophys. J.* **2004**, *86*, 435–447.

Studies involving NO binding to a variety of mutants at position 68 have also been reported,<sup>28,38,97</sup> and it was suggested that the slow phase of the geminate rebinding involved the return of the ligand from the Xe4 cavity and/or other parts of the interior distal pocket.

The experiments presented here are the first direct kinetic measurements of the temperature-dependent NO recombination to the heme iron in Mb. Different heme environments have been examined, including the wild type, the V68 mutants, and the protoheme (with the distal pocket and proximal histidine removed). The novel methodology developed to perform these studies allows us to compare the temperature dependence of the NO recombination in these samples. The temperature-dependent data demonstrate that the enthalpic barrier for NO rebinding to the heme is negligible, whereas the escape of NO from a more distant site (probably the Xe4 cavity) involves a barrier on the order of 3 kJ/mol. Other information concerning the relaxation of the distal protein pocket, and the effect of the proximal imidazole bond and heme doming on the NO binding reaction, is also deduced from this work.

### Experimental Methods

**Sample Preparation.** Horse-heart myoglobin (Mb) was purchased from Sigma Chemical Co., used without further purification, and prepared in 75–80% glycerol (v/v) potassium phosphate buffer (pH = 7.8, 0.1 M). The samples are prepared in a glovebox under argon atmosphere to prevent unwanted contamination from molecular oxygen. Under these conditions, 4  $\mu$ L of 1 M sodium dithionite ( $\text{Na}_2\text{O}_4\text{S}_2$ ) solution is added to 300  $\mu$ L of buffered sample to obtain the deoxy (reduced) Mb species. An additional 2  $\mu$ L of 1 M  $\text{NaNO}_2$  solution is added to prepare the MbNO adduct. The concentration of protein is chosen so that the sample has an absorbance of about 1 optical density (OD) at the pump wavelength in a 1 mm path length cell. The ferric V68W and V68F mutants were provided by Professor John Olson (Rice University). The preparation of the NO adduct of the mutant samples was done using the same procedure as that for the wild-type (wt) myoglobin sample. Sperm whale Mb, obtained from Sigma Chemical Co., was also carefully compared to horse-heart Mb.

Ferric protoporphyrin IX chloride (hemin) was purchased from Porphyrin Products Inc., dissolved in 1 M NaOH, and then diluted into glycerol. For typical 80% (v/v) glycerol solutions (glycerol obtained from Acros Organics), the final sample pH is 12. The hemin concentrations for kinetics measurements are typically 50–100  $\mu$ M. At higher heme concentration in glycerol solution, aggregation is observed, as evidenced by the blue shift of the Soret and the red shift of band III in the deoxy sample spectra.<sup>102</sup> After flushing with argon, the sample is reduced by addition of a small amount of degassed sodium dithionite solution. The NO adduct is formed from the reduced sample by adding 2  $\mu$ L of 1 M  $\text{NaNO}_2$  solution. The equilibrium absorption spectra of the samples are obtained using a Hitachi U-3410 spectrophotometer.

Following preparation, the sample is transferred to a homemade cryogenic gas-tight sample holder under  $\text{N}_2$  atmosphere. The sample is in direct contact with the gold-plated copper sample holder to ensure a good heat transfer between the sample and the cryostat coldfinger. The sample holder is transferred into the optical cryostat (Janis Research, CCS-150), and after a 1 mTorr vacuum guard is achieved (to minimize heat transfer through the surrounding air), the cooling process is started at a rate of 3 K/min. The temperature is controlled by a model 331E Lakeshore temperature controller, and the temperature readings are made by two matched silicon diode temperature sensors, one installed at the control heater and the other one installed at the

bottom of the sample holder. After the readings from the two temperature sensors reach the desired temperature, the sample is thermally equilibrated at this temperature for about 30 min before the measurements are taken.

**Laser System.** The laser system used for these experiments consists of a Ti/Sapphire self-mode locked resonator (MIRA, Coherent, Inc.) that generates tunable (between 700 and 960 nm) femtosecond pulses (60–100 fs) with a repetition rate of 76 MHz, each containing about 10 nJ of energy.

The blue pulses needed to pump and probe the sample in the Soret absorption band are obtained by doubling the IR light using a 0.25 mm BBO crystal, after which the pulses are chirp compensated by a pair of SF10 prisms to about 5–8% of the transform limit time-bandwidth product. After compression, the pulse train is passed through a pulse modulator or a “pulse picker” (Conoptics, Inc.) to lower the repetition rate of the laser (typically by a factor of 20) to help overcome the possibility that, at certain lower temperatures, the recombination rates might slow and become competitive with the repetition rate of the laser. The laser system was tuned into resonance with the product state of the studied sample, five-coordinate, histidine ligated, deoxy Mb at 433 nm and weakly five-coordinated (i.e., with water)  $\text{Fe}^{2+}$ PPIX in 80% glycerol at 423 nm.

**Signal Processing.** Because of the small absorption changes that occur when the pump beam excites the sample and the need for a good signal-to-noise ratio, a cascaded lock-in amplifier technique is used where both the pump and probe beams are modulated so that the pump-induced change in the sample transmission can be monitored by detecting a probe-modulated signal. The pump beam is modulated by a Neos Technologies acousto-optic modulator (AOM) at 1.5 MHz, and the probe beam is modulated by a mechanical chopper working at approximately 800 Hz. The pump beam is passed through an optical delay line with a motorized translation stage (Newport, translation range  $\sim$ 1.2 ns) that controls the pump–probe time delay. Special care was taken in aligning the translation stage using a photodiode and a 50  $\mu$ m pinhole system that traveled along with the translation stage and gauged the collimation and parallelism of the laser beam. The beams are collimated into a parallel geometry so that spatial filtering of the pump beam is possible. The polarizations of the pump and probe pulses are also set to be perpendicular to improve the rejection of pump leakage into the detector.

We use the double-modulation technique<sup>80,103</sup> as a third method to reject the pump light leakage into the signal channel. The leakage is especially problematic in low-temperature experiments because of the inherent light scattering in the frozen sample, which leads to poor spatial and polarization separation of the pump and probe beams (the polarizations are lost because of multiple scattering and stress-induced polarization scrambling).

The dual cascaded lock-in amplifier (LIA) method is configured to detect only the pump-induced and probe-modulated transmission signals. The high-frequency lock-in (from which the reference signal for the AOM is derived) is set to have a large bandwidth so that the low-frequency probe-modulated signal can pass and be detected by a second lock-in (from which the reference signal for the mechanical chopper is derived). An appropriate choice of LIA time constants and chopping frequencies must be employed to minimize the noise level transmitted within the bandwidth of the first LIA. Typical settings for the experiments reported here are as follows: the high-frequency lock-in that generates the driving AOM frequency is 1.5 MHz with the detection time constant set at  $t = 100 \mu$ s (corresponding to a 24 dB/oct equivalent noise bandwidth, ENBW, of 781.2 Hz = 5/64T), whereas the second, low-frequency LIA is set to work at 0.8 kHz with the detection bandwidth set at 300 ms (ENBW = 260.4 mHz).

**Sample Scanning.** Sample rotation is a common approach that is often used with pulsed laser systems to avoid sample deterioration.

(102) Ye, X.; Yu, A. C.; Georgiev, G. Y.; Gruia, F.; Ionascu, D.; Cao, W. X.; Sage, J. T.; Champion, P. M. *J. Am. Chem. Soc.* **2005**, *127*, 5854–5861.

(103) Ionascu, D.; Gruia, F.; Rosca, F.; Yu, A.; Champion, P. M. To be submitted, 2005.

Also, thermal lensing can give rise to a time-varying signal at the pump beam modulation frequency and create an undesirable large background signal, which is also eliminated by spinning the sample. Unfortunately, there are experimental situations (cryogenic studies are one of them) where the sample is required to be stationary.

To overcome the problems associated with the stationary sample requirement in low-temperature experiments, we developed a novel fast-scanning technique<sup>103</sup> based on an off-axis spinning lens that creates a common focal point moving in a circle of adjustable radius (1–4 mm). We also found that sample centrifugation (6g) for about 10 min significantly reduced the number of cracks within the formed glass. When a suitable sample has been prepared, the radius can be adjusted so that the circular path of the pump and probe beams does not encounter cracks in the sample. The details of the technique will be described elsewhere.<sup>103</sup> Briefly, the methodology allows us to probe stationary samples at cryogenic temperatures and helps to minimize the thermal lensing background signals. Following the sample, a collection lens is used to image the light from the pump and probe beams, after which the pump and probe beams are spatially separated using a pinhole and a polarization analyzer. Even though the double modulation ensures a background free signal without pump leakage, we use the polarization selection to minimize the nonlinear mixing of the modulation frequencies within the detector. This effect occurs because of the nonlinearity of the detector when the average laser power rises above 5 mW, which can create an undesired mixing of the pump- and probe-modulation frequencies that gives rise to a constant background. The nonlinear mixing was tested by monitoring the dc background signal as a function of the attenuation of the pump and probe beam intensities. The detector used was a biased silicone pin photodiode (Thorlabs, Hamamatsu).

**Data Analysis.** The analysis of the rebinding kinetics is carried out using the maximum entropy method<sup>104,105</sup> algorithm. The maximum entropy method (MEM) does not make any preanalysis assumptions and therefore does not imply any time domain model of choice but rather seeks a representation for the recombination process in the space of decay rates. We can write the survival probability of the unbound ligands as

$$N(t) = \int_0^{\infty} g(\lambda) e^{-\lambda t} d\lambda$$

where  $g(\lambda)$  is the rate distribution of the recombination process. When the kinetics stretches over several decades of time, the rate space is conveniently redefined to a logarithmic rate space. The MEM algorithm is used to extract the rate distribution which, for a typical ligand rebinding process, presents several peaks that are usually attributed to particular dynamic processes or conformational substates. To ensure the accuracy of peak estimation, the rates are extracted by taking the derivative of the rate distribution. However, for some particular cases, the rate distribution does not present distinctly well-defined peaks so we sometimes approximate the resulting rate distribution with a Gaussian least-squares fit using the Levenberg–Marquardt algorithm.<sup>106</sup> For the MbNO kinetics reported here, we use two Gaussians to fit the MEM distribution to approximate the relative amplitudes of the two kinetic processes. The errors associated with this procedure can be relatively large and systematically depend on the separation between the kinetic phases. The errors in the slower-phase amplitude increase at lower temperatures because the Gaussian fit to the long time tail of the time-constant distribution begins to deteriorate.

Subsequently, the data are fit using other models, sometimes using the MEM results as the initial guess. We have tried various combina-

tions of fitting functions, and we find that an exponential for the fast phase and a stretched exponential for the slow phase do a reasonable job approximating the data. Generally, we use the Levenberg–Marquardt algorithm for nonlinear least-squares fitting, and we find that the data are not well fit using the standard exponential fitting functions. On the other hand, the use of the MEM algorithm ensures an unbiased approach to the data analysis, as demonstrated by earlier studies.<sup>96,105,107</sup> With this in mind, we emphasize that time-dependent rate processes, due to relaxation effects, cannot be differentiated from a static distribution of rates simply by applying a MEM analysis (MEM will fit both processes equally well). Additional experimental techniques, such as double pump-pulse kinetic selection,<sup>72</sup> must be used to decide if the ensemble is kinetically inhomogeneous or if barrier relaxations are present.

In the course of these investigations, we also found that the MEM technique can have significant difficulties in extracting the underlying rate distribution when a stretched relaxation is present that cannot be followed over its full dynamic range.<sup>108</sup> As a result of this problem, the MEM data analysis yields a slow kinetic phase with a rate process that appears to level off below ~100 K. This arises from the fact that the experimental arrangement used in these studies cannot follow the kinetics beyond ~1200 ps. Because the slow-phase kinetics are stretched, the MEM peak does not continue moving toward longer time constants when the slower portion of the decay begins to extend beyond the experimentally accessible time window below ~100 K. Therefore, as an alternative fitting procedure below 100 K, we utilized an exponential plus a stretched exponential to fit the data. Using this approach, we confirmed that the underlying kinetic time scale of the slow phase continues to increase as the temperature is lowered below 100 K, consistent with an Arrhenius barrier on the order of  $3 \pm 1$  kJ/mol. A similar problem involving missing MEM amplitude appears for the slow phase, but the alternative fitting procedure suggests that the relative amplitudes remain fixed. As a result, the areas of the two independently normalized Gaussian fits to the MEM data, which do tend to remain constant, are plotted in Figure 2 (i.e., the sum of the two Gaussian areas is not forced to remain invariant at all temperatures). The large error bars reflect the uncertainties associated with the MEM analysis and the limited experimental time window.

## Results

The ultrafast studies of MbNO demonstrate that, upon photodissociation, the rebinding kinetics partitions into two phases, with distinctly different temperature dependence. Kinetic studies only at room temperature do not allow an unequivocal distinction of the two phases to be made. This is because at room temperature the two kinetic phases are only separated by a single decade in time, and nonexponential relaxation models can be used to approximate the response within the context of a single kinetic phase. The use of glycerol to control the viscosity at room temperature indicates that two phases are present when MEM analysis is employed,<sup>96</sup> but does not completely rule out alternative relaxation models that invoke a single kinetic phase. On the other hand, Figures 1 and 2 demonstrate that one of the phases (the fast phase) maintains a nearly constant rate  $\sim 10^{11}$  s<sup>-1</sup> over the entire range of studied temperatures, whereas the other kinetic phase (the slow phase  $\sim 10^{10}$  s<sup>-1</sup> at  $T = 200$  K) slows down as the temperature is lowered. Thus, in Figure 1, we can clearly differentiate the two phases at low temperature and unambiguously assign them as separate kinetic processes independent of the details of a specific fitting approach.

Because there is a natural break in the kinetic response as a function of temperature near the glass transition temperature

(104) Skilling, J.; Bryan, R. K. *Mon. Not. R. Astron. Soc.* **1984**, *211*, 111.

(105) Kumar, A. T. N.; Zhu, L.; Christian, J. F.; Demidov, A. A.; Champion, P. M. *J. Phys. Chem. B* **2001**, *105*, 7847–7856.

(106) Press, W. H.; Teukolsky, S. A.; Vetterling, W. T.; Flannery, B. P. *Numerical Recipes in C*, 2nd ed.; Cambridge University Press: New York, 1992.

(107) Steinbach, P. J. *Biophys. J.* **1996**, *70*, 1521–1528.

(108) Ionascu, D. Ph.D. Thesis, Northeastern University, 2005.

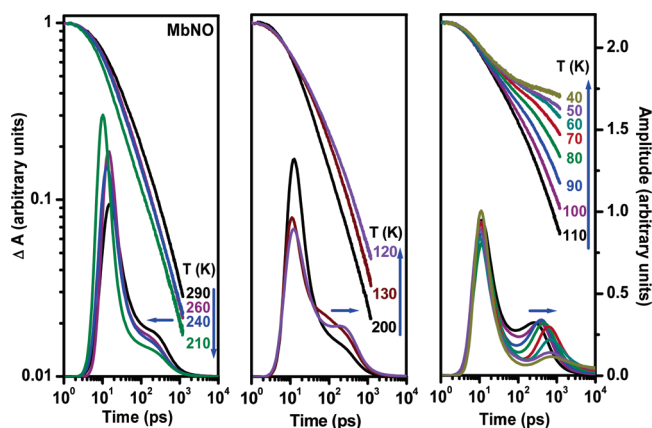


**Figure 1.** MbNO temperature-dependent NO recombination dynamics to myoglobin after photolysis. The MEM inverse rate distributions along with the time evolution of the sample absorption change are shown for clarity on a double logarithmic scale. The MEM amplitudes are measured linearly on the right axis. Vertical and horizontal arrows indicate the kinetics tendency and the slow-phase rate tendency, respectively, as the temperature is lowered from 290 to 40 K. The left panel demonstrates the anomalous temperature-dependent behavior where the recombination process is speeding up as the temperature is lowered toward 210 K.

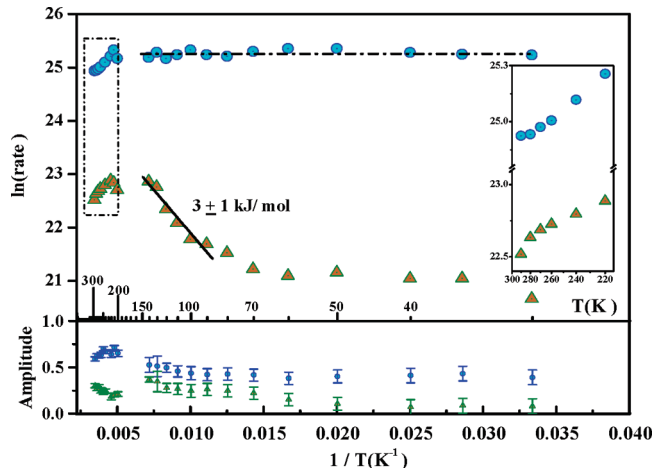


**Figure 2.** Upper panel presenting the natural logarithm of MEM extracted rates as a function of inverse temperature (Arrhenius plot  $\ln(k)$  vs  $1/T$ ) along with the corresponding independently normalized rate amplitudes (lower panel) for MbNO. The barrier associated with the slow process (triangles) is found to be  $3.0 \pm 1$  kJ/mol. The fast process is found to be independent of temperature with no barrier. The upper panel inset resolves the temperature region between 290 and 220 K (dashed rectangle) in which the recombination becomes faster as the temperature is lowered.

( $T_g \sim 180$  K in the 80% glycerol/water solvent), we divide the kinetic responses into separate temperature ranges, as shown in Figure 1. The MEM distributions (translated from rates to time constants;  $\tau = k^{-1}$ ) are shown in the lower part of Figure 1, where it can be seen that both phases slow slightly above 200 K. Below 200 K, the slow phase gets slower as the temperature is lowered and the fast phase is independent of temperature. The former observation indicates that an enthalpic barrier is associated with the slow kinetics process below  $T_g$ , and the latter demonstrates that no enthalpic barrier is present for the fast phase. The temperature dependence above  $T_g$  suggests that some type of protein relaxation is taking place as the surrounding solvent softens and melts.

In the region of the solvent glass transition (150–200 K), the optical quality of the samples deteriorates and it appears that a small decrease and recovery of the kinetic rate constants

takes place. However, because of the poor optical quality of the samples near  $T_g$  and the associated noise in the kinetic data, we have not included these results in Figure 2. At the lowest temperatures (right-hand panel of Figure 1), the sample is completely frozen and the ligand rebinding can be followed from 130 to 30 K. In this temperature regime, the slow kinetic phase moves away from the fast phase so that it can be more clearly delineated. For consistency and clarity in the presentation of the kinetic data and the MEM rate distributions, we use the same format as that in Figure 1 to present the NO rebinding kinetics of the distal pocket Mb mutant (V68W) and the “bare” heme model compound (PPIX).

In Figure 1, the temperature-dependent rebinding kinetics of MbNO are plotted using the logarithm of the normalized absorption  $\Delta A$  as a function of logarithmic time. The vertical arrows indicate the direction of the kinetic response as the temperature is lowered. The horizontal arrows indicate how the slow-phase MEM time-constant distribution changes as the temperature is decreased. The MEM time-constant distributions are shown using the same logarithmic time axis that is used for the kinetics, but with a linear amplitude that is given on the right axis.

As can be clearly seen in the left panel of Figure 1, the recombination kinetics shows anomalous behavior as the temperature is lowered from 290 to 200 K, becoming faster (rather than slower) as the temperature is decreased toward the solvent glass transition. This anomalous temperature dependence above 200 K is observed for both phases (Figure 2, upper panel and inset). Below 200 K, the slower phase (which appears as a shoulder on the faster-phase rate distribution) behaves normally and its rate distribution slows down as the temperature is decreased (see horizontal arrows in the middle and right panels of Figure 1 and in the Arrhenius plots of Figure 2). It is noteworthy that the amplitudes of the two phases shown in the lower panel of Figure 2 remain roughly constant as the temperature is varied. The amplitudes are found by fitting the MEM rate distributions in Figure 1 using two Gaussian functions, which leads to a relatively large error in the amplitude determination, particularly for the slow phase at lower temperatures (as determined by the increasing difference between the integrated areas of the unnormalized Gaussian fits and the MEM distribution).

As can also be seen in Figure 2, the fast-phase time constant is independent of temperature below the glass transition. The rate change for the slow phase (triangles in the upper panel of Figure 2) leads to an enthalpic barrier of  $3 \pm 1$  kJ/mol between 80 and 200 K, but appears to level off below 80 K. As mentioned in the Experimental Methods section, the leveling off effect is probably an artifact that arises when the long time tail of the nonexponential slow-phase kinetic response begins to move beyond the experimental detection window (1.2 ns) at lower temperatures. Separate fits to the data in this region using an exponential for the fast phase and a stretched exponential for the slow phase<sup>108</sup> were therefore used (along with the MEM analysis between 80 and 200 K) to help establish both the errors and the magnitude of the enthalpic barrier for the slow phase.

In Figure 3, we contrast the room-temperature MbNO rebinding kinetics of wild-type (wt) whale (SW) and horse (HH) along with two of the SW mutants (V68F and V68W). Both a pure aqueous buffer solution and a 75% glycerol/water mixture were used for solvent. The left panel shows the samples in water,

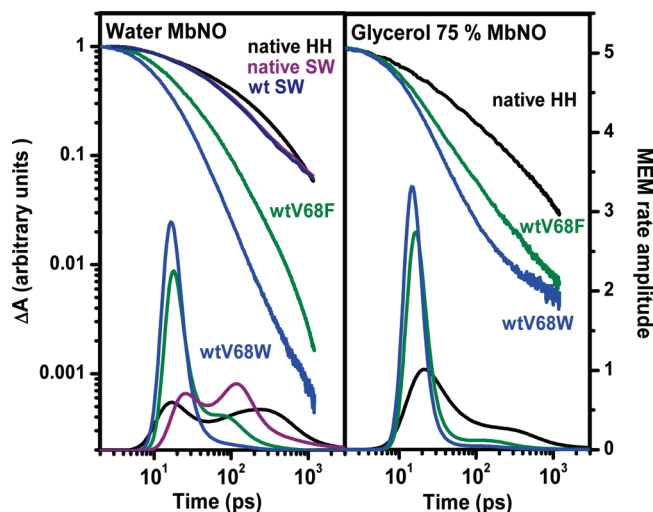


**Figure 3.** NO recombination dynamics to wt Mb, SW Mb, HH Mb, Mb(V68F), and Mb(V68W) mutants in aqueous buffer (left panel) and 75% glycerol buffer (right panel). The MEM amplitudes are measured linearly on the right scale. Note the relatively dramatic slow-phase amplitude decrease that appears with glycerol-based solvent or V68 mutations.

and the right panel shows the samples in 75% glycerol solution. Note that there are small species differences observable in the kinetics response of the slow phase; however, these are small effects in comparison to the mutations at V68, so we do not focus on them here. The native and wt SW Mb have a virtually identical kinetic response, and they cannot be differentiated in the figure.

The V68 mutants are important because of the fact that the distal valine-68 is adjacent to the ligand-binding site and resides along the pathway to the Xe4 pocket where it can play a potentially important role in determining the overall kinetic barrier to ligand binding<sup>27,50,99</sup>. There are two major experimental observations to be emphasized in Figure 3. First, there is a dramatic decrease in the slow-phase amplitude when the native MbNO is either mutated at V68 (F or W) or if the solvent environment is changed by adding glycerol. Second, and perhaps most important, is the observation that the fast phase is nearly independent of both the solvent environment and the sample mutation. The dramatic decrease of the slow-phase amplitude when glycerol is added agrees quantitatively with an earlier report by Shreve et al.,<sup>96</sup> which showed a systematic decrease in the slow-phase amplitude, along with a small increase in the slow-phase rate, as the glycerol concentration in the MbNO samples was increased.

In Figure 4, we plot the temperature-dependent NO recombination kinetics of the V68W mutant. The analysis reveals only a single fast phase with an Arrhenius rate behavior, shown in Figure 5. The kinetics is nearly identical to the behavior observed for the fast recombination phase found in wild-type MbNO, including the weak relaxation and slowing down of the rate as the temperature is increased from 200 to 290 K. Remarkably, the rebinding rate has essentially no temperature dependence in the V68W mutant and the second (slow) phase is almost completely suppressed. However, at the lowest temperatures, a slow phase of the kinetic response becomes barely detectible, reflecting the presence of a very small component of this phase (note that the amplitude of this phase is much smaller than that in the wild type because the vertical logarithmic axis for the rebinding kinetics in Figure 4 includes

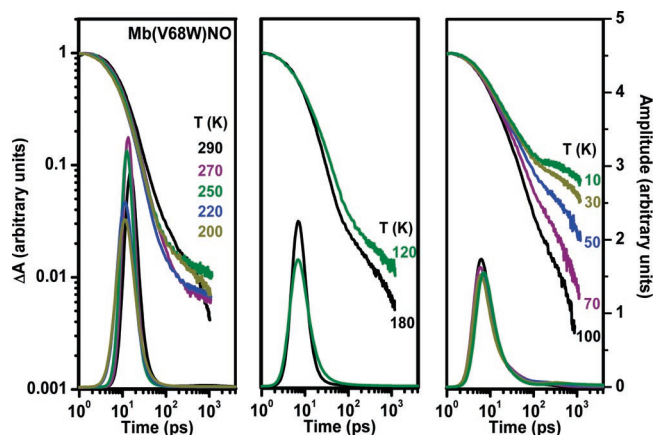


**Figure 4.** Temperature-dependent NO recombination following photolysis of Mb(V68W)NO in glycerol-based (75%) buffer plotted along with the corresponding maximum entropy distribution.

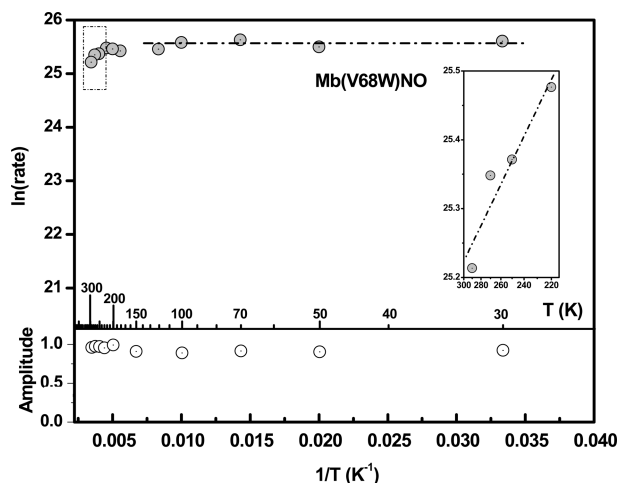


**Figure 5.** Mb(V68W)NO.  $\ln(k)$  vs  $1/T$  (upper panel) and the corresponding MEM rate amplitudes as a function of temperature (lower panel). The upper panel inset resolves the temperature region between 290 and 220 K (dashed rectangle) in which the recombination becomes faster as the temperature is lowered.

an extra decade compared to that in Figure 1). Evidently, the single-phase ultrafast kinetic response of the V68W mutant provides a clean experimental look at NO rebinding to the heme from the distal pocket of Mb without complications associated with ligand migration to other parts of the protein.

Similar temperature-dependent kinetic measurements have been performed on samples of NO-ligated PPIX in glycerol, as shown in Figures 6 and 7. Again, we find that temperature-independent rate behavior is observed below the solvent glass transition. The role of the protein environment that surrounds the heme is revealed by the kinetics between 200 and 290 K. In contrast to the Mb samples, the kinetics of NO rebinding to bare heme (with water as the fifth ligand) does not slow as the temperature is increased over this temperature range. Instead, the rates tend to increase (very gradually) with temperature and the Arrhenius plot (see inset in Figure 7) indicates a small enthalpic barrier ( $\sim 0.3$  kJ/mol) in the temperature range above  $T_g$ . Given the absence of both the imidazole ligand and the protein material, it is not surprising that the heme in the PPIXNO samples may go through a conformational relaxation process different from that observed for MbNO.

Finally, in Figure 8, we display the Soret band evolution for the MbNO sample at room temperature, obtained using a white



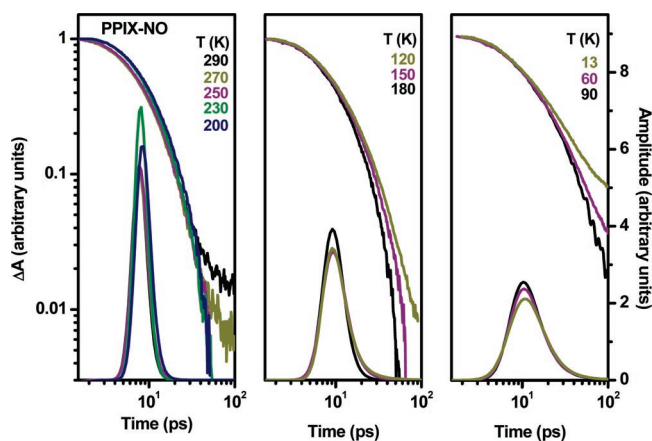


**Figure 6.** PPIXNO temperature dependence of NO molecule recombination following photolysis of PPIXNO in 80% (v/v) glycerol solution plotted on a log–log scale along with the corresponding maximum entropy distribution.

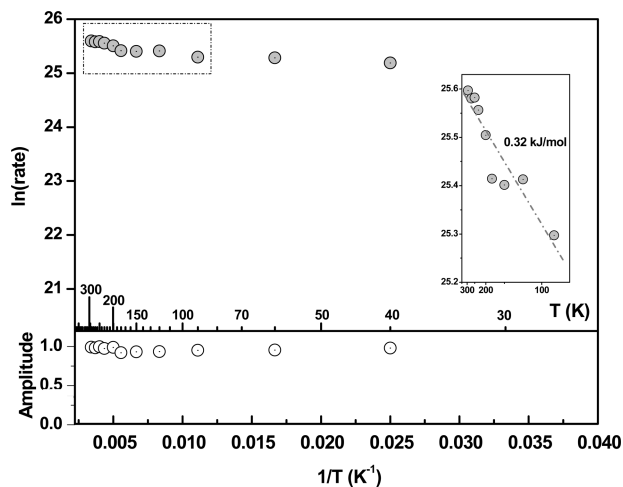


**Figure 7.** PPIXNO plot of  $\ln(k)$  against inverse temperature. The inset resolves temperatures from 290 to 90 K, revealing a barrier of 0.32 kJ/mol. The lower panel shows the rate amplitudes to be constant over all the studied temperature ranges.

light continuum spectrometer.<sup>15</sup> Because NO binding to imidazole-ligated heme systems can lead to the rupture of the imidazole bond, it is important to clearly establish the state of the proximal histidine–iron bond in the MbNO system (both in equilibrium and immediately following NO photolysis). This issue is important because the time scale for NO rebinding is  $\sim 10$  ps for both the PPIXNO (no imidazole) and the fast component of the MbNO samples. The similarity in the rebinding rates could potentially indicate that the histidine bond is (transiently) absent in the Mb sample. However, as can be seen from the equilibrium and dynamic Soret band difference spectra in Figure 8, there is a prompt appearance of the five-coordinate (histidine-ligated) deoxy Mb spectrum (peaking at 435 nm) upon NO photolysis. If the histidine ligand was lost, one would expect to see evidence of a transient bleach near 390 nm, analogous to the Soret spectra of the water-ligated PPIXNO, as shown in the lower portion of Figure 8. However, the 390 nm spectral signature is absent and a normal “hot” (broadened and slightly red shifted<sup>109</sup>) deoxy Soret band at 435 nm is clearly present in the early time window. Moreover, femtosecond coherence

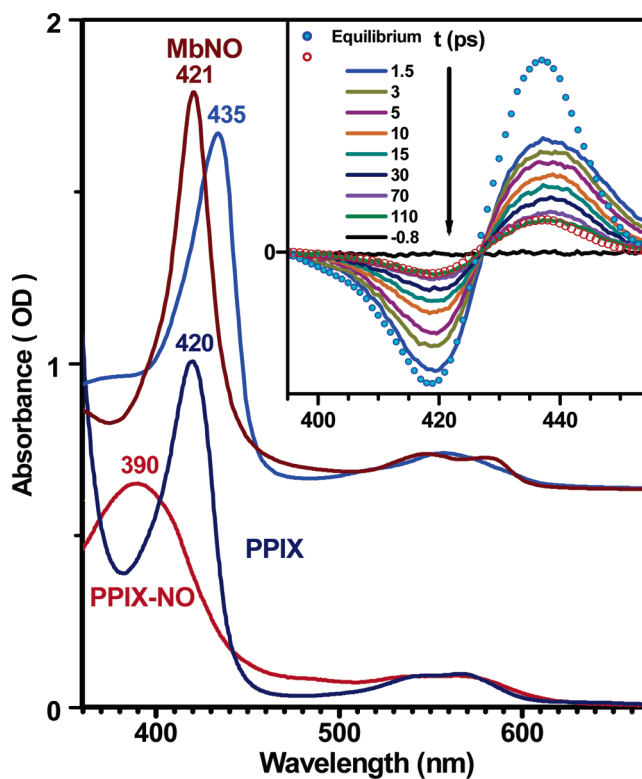


**Figure 8.** Absorption spectra before and after the photolysis of the MbNO and PPIXNO at room temperature. The inset shows the MbNO transient difference spectra at different times. The spectra demonstrate the photolysis-induced formation of five-coordinated iron species (histidine-ligated deoxy Mb) at 435 nm with no sign of a bleach at 390 nm, characteristic of the PPIXNO system in the absence of a histidine ligand. The blue and red circles depict the renormalized equilibrium difference spectrum of Mb and MbNO, which is well approximated by the transient difference.

spectroscopy studies on MbNO have revealed that, upon photodissociation, the  $220\text{ cm}^{-1}$  vibrational coherence of the iron–histidine stretching mode appears nearly instantaneously ( $\ll 150$  fs),<sup>80,81</sup> further validating that the iron–histidine bond is intact. These results demonstrate that the proximal histidine remains ligated to the heme in Mb, both when NO binds and immediately after it is photodissociated from the heme.

## Discussion

**Barriers.** This work presents the first systematic investigation of the effect of temperature on the ultrafast rebinding of the NO ligand to heme proteins. Several of the main experimental observations are emphasized in Table 1, which displays some of the time constants and barriers for the various samples near room temperature (290 K) and just above the solvent glass transition (220 K). The faster of the two kinetic phases in MbNO shows a time constant of  $\sim 15$  ps at 290 K that decreases to  $\sim 12$  ps (i.e., the rate increases) as the temperature is lowered to 220 K. This same trend (i.e., a small decrease in the observed kinetic rates as the temperature is raised above  $T_g$ ) is observed in all of the protein samples studied. Such anomalous kinetic behavior signals that a protein relaxation process is taking place in the temperature range above  $T_g$ . In contrast, when the temperature is decreased below 220 K, the time constant of the fast phase remains fixed, signifying an enthalpic barrier that is negligible for this kinetic process. For the slow phase, the rate decreases when the temperature is lowered below  $T_g$ , as normally expected, so we report the Arrhenius barrier of the

(109) Ye, X.; Demidov, A.; Rosca, F.; Wang, W.; Kumar, A.; Ionascu, D.; Zhu, L.; Barrick, D.; Wharton, D.; Champion, P. M. *J. Phys. Chem. A* **2003**, *107*, 8156–8165.

**Table 1.** Kinetics Fitting Parameters for Selected Hemes and Heme Proteins

sample	fast phase				slow phase <sup>a</sup>			
	$T = 290$ K	$T = 220$ K	relaxation barrier <sup>c</sup> (kJ/mol)	Arrhenius barrier (kJ/mol)	$T = 290$ K	$T = 220$ K	relaxation barrier <sup>c</sup> (kJ/mol)	Arrhenius barrier (kJ/mol)
	$k$ (s <sup>-1</sup> ) $\tau^b$ (ps) amplitude (%)	$k$ (s <sup>-1</sup> ) $\tau^b$ (ps) amplitude (%)			$k$ (s <sup>-1</sup> ) $\tau^b$ (ps) amplitude (%)	$k$ (s <sup>-1</sup> ) $\tau^b$ (ps) amplitude (%)		
MbNO (80% gly)	$6.8 \times 10^{10}$ 15 68	$9.0 \times 10^{10}$ 11 80	0.7	$0 \pm 0.2$	$6.0 \times 10^9$ 170 32	$8.7 \times 10^9$ 115 20	0.9	$3 \pm 1$
(V68F)NO (75% gly)	$9.0 \times 10^{10}$ 11 88				$1.1 \times 10^{10}$ 91 12			
(V68W)NO (80% gly)	$9.0 \times 10^{10}$ 11 99	$1.2 \times 10^{11}$ 8.6 99	0.6	$0 \pm 0.2$				
PPIXNO <sup>d</sup> (80% gly)	$1.3 \times 10^{11}$ 7.7 99	$1.2 \times 10^{11}$ 8.3 99	0	$0.3 \pm 0.1$				
MbNO (water)	$8.4 \times 10^{10}$ 12 40				$5.0 \times 10^9$ 200 60			

<sup>a</sup> Another small slow-geminate phase near 1 ns is resolved in longer-scan kinetic data but is not resolved in the 1.2 ns scan-range data analyzed here. This could lead to small systematic errors in the slow-phase parameters given in the table. <sup>b</sup> The rates and amplitudes are found from Gaussian fits to the MEM distributions. The errors are estimated to be  $\sim 5\%$  for the rates and 10–15% for the amplitudes. <sup>c</sup>  $-2.42 \ln[k_{290\text{K}}/k_{220\text{K}}]$ . <sup>d</sup> No added imidazole.

slow phase below  $T_g$  to unambiguously separate it from the relaxation process above  $T_g$ .

As can be seen in Table 1, the enthalpic barrier for the slow kinetic phase in MbNO is  $\sim 2$ – $4$  kJ/mol and the amplitude of this phase is significantly reduced (V68F) or eliminated (V68W) by distal pocket mutants that block the Xe(4) binding site.<sup>50,99</sup> As a result, we assign this kinetic process to movement of the NO ligand from a site in or near the Xe4 pocket, following its partial population by hot photolyzed [NO]<sup>\*</sup> ligands (see Scheme 2). Within the context of Scheme 2 (with  $k_{XA} = 0$ ), the Arrhenius barrier extracted for the slow kinetic phase can be assigned directly to the transition from state “X” (in or near the Xe4 pocket) to state “B” (the heme localized distal pocket). The amplitude of the kinetic phase associated with the transition from state X to B can also be increased by choosing a more energetic photon for photolysis (see following). Finally, we note that there is a small increase of the fast-phase rate constant when the NO rebinding kinetics of the V68W mutant is compared to wt Mb. We attribute this effect to a somewhat smaller ligand-accessible volume in the distal pocket (B state) of the V68W mutant.

**Viscosity.** In agreement with the work of Shreve et al.,<sup>96</sup> we find that the addition of glycerol leads to a systematic reduction of the slow-phase amplitude without a significant change in its rate. The lower panel of Figure 2 also indicates that the slow-phase amplitude decreases and the fast-phase amplitude increases as the temperature is lowered from 290 to 220 K. Because the effect of both the addition of glycerol and the decrease of temperature in the 290–220 K range is to increase the solution viscosity, we suggest that increased viscosity is an important cause of the decrease in the amplitude of the slow kinetic phase. This may be due to the damping of key protein fluctuations, which enable the transitions of the NO ligand from the localized distal pocket (B state) into the region of the more distant Xe4 cavity (X state).

On the other hand, we note that glycerol has the potential to perturb the protein structure<sup>110,111</sup> and, if a more “open” protein structure is induced by the addition of glycerol, partial oc-

cupancy of the Xe4 pocket by glycerol or water may be possible. Near the solvent glass transition at 200 K, and below, the amplitudes extracted from the MbNO rebinding kinetics also show variation, but this is probably due to significant systematic errors in extracting the amplitudes at the lower temperatures (see Experimental Methods section). In addition to the loss of slow-phase amplitude when the kinetics moves beyond the allowed ( $\sim 1$  ns) experimental time range, the errors are increased because the MEM distributions describing the kinetics are not always well fit using two symmetric Gaussians.

**Relaxation.** The slowing down of the kinetics that occurs at higher temperatures evidently arises from the initial relaxation of the photolyzed freeze-quenched MbNO protein structure toward the deoxy Mb protein conformation as the temperature is raised above  $T_g$ . The effect of this relaxation on the MbNO kinetics is relatively small and is approximated in Table 1 by using the ratio of observed rates at 290 and 220 K. The logarithm of this ratio can be used to approximate the increment in the free-energy barrier,  $\Delta G_{\text{relax}}$ , that would be needed to account for the anomalous rate decrease with increasing temperature. (The approximation holds exactly for the fast phase, where the enthalpic barrier is zero at 220 K.) It is noteworthy that the magnitude of the relaxation, as quantified by  $\Delta G_{\text{relax}} \sim 0.6$  kJ/mol, is nearly the same for all of the protein samples studied. In contrast, the model heme compound (PPIXNO in glycerol) displays no relaxation process above  $T_g$ , even though the fast rebinding time constant ( $\sim 8$  ps) is close to what is observed ( $\sim 12$  ps) in the protein prior to the onset of relaxation. The absence of an enthalpic NO rebinding barrier for the fast kinetic phase of MbNO and PPIXNO below 200 K suggests that the protein relaxation process observed above 200 K is most likely associated with small entropic changes. One possibility is that the increasing degrees of freedom available to the protein at

(110) Sivakolundu, S. G.; Mabrouk, P. A. *J. Am. Chem. Soc.* **2000**, *122*, 1513–1521.

(111) Sivakolundu, S. G.; Mabrouk, P. A. *J. Biol. Inorg. Chem.* **2003**, *8*, 527–539.

higher temperatures lead to a “softening” of the deoxy Mb protein structure, with a concomitant increase in the ligand accessible volume(s) of the distal pocket(s).

It has also been suggested<sup>30,84</sup> and contested<sup>38,39,112,113</sup> that evolution in the local heme structure (i.e., time-dependent changes in the iron out-of-plane displacement) may be responsible for the nonexponential nature of the geminate kinetic response in MbNO. However, the clear separation of the kinetics into a fast exponential phase and a slower phase at lower temperatures, along with the crossover to essentially single exponential ( $\sim 10$  ps) behavior when the Xe4 pocket is blocked, suggests that a time-dependent geometric change of the heme is an unlikely explanation for either the nonexponential kinetics at room temperature or the small  $\sim 0.6$  kJ/mol relaxation seen in the MbNO binding reaction. As a result, we do not consider further the possibility of a time-dependent heme barrier and  $k_{\text{BA}}$  is taken to be constant in the kinetic schemes presented below.

In contrast to the NO rebinding results, the temperature-dependent kinetics studies of CO binding to both PPIX<sup>60,114</sup> and Mb display a much more significant decrease in the rate of ligand rebinding as the temperature is increased from 220 to 290 K. The  $\sim 3$  kJ/mol ( $T > T_g$ ) relaxation observed in the CO rebinding reaction for PPIXCO<sup>114</sup> and the even larger relaxation of  $\sim 10$  kJ/mol for MbCO<sup>102</sup> evidently do arise from changes in the heme geometry (e.g., increased doming) that take place as the protein evolves from the six-coordinate ligand-bound conformation to the fully relaxed five-coordinate deoxy conformation.<sup>85,102,115,116</sup> This view is also consistent with the fact that the enthalpic rebinding barrier for MbCO is much larger ( $\sim 10$  kJ/mol)<sup>102</sup> than that for MbNO ( $\sim 0$  kJ/mol) below 220 K. Overall, the kinetic results suggest that, when CO binding is used as the kinetic probe molecule, the heme geometric changes induced by the protein relaxation at higher temperatures will be important. The heme structural relaxation acts to increase the enthalpic rebinding barrier for CO (but not NO) as the solvent/protein/heme system relaxes from the ligand-bound to the ligand-unbound conformation.<sup>114</sup>

**Kinetic Inhomogeneity.** Understanding why the rebinding barrier at the heme is significantly larger for CO than for NO has been a long-standing question.<sup>28,117</sup> To this, we must now add the observation that the low-temperature rebinding kinetics for MbCO shows extremely nonexponential (i.e., highly stretched) behavior,<sup>18</sup> and for MbNO (wild type and V68W), the fast-phase kinetics is well described by an exponential process. The exponential behavior of the MbNO kinetics is quite surprising because a well-accepted reason for the stretched kinetics of MbCO is that the protein conformational substates are “frozen out” on the time scale of the CO rebinding process.<sup>18,24,71,118</sup> At higher temperatures (above  $T_g$ ), the conformational substate interconversion rates begin to exceed the CO rebinding rates; thus, the kinetic inhomogeneities are averaged, and the CO rebinding barrier at the heme becomes nearly exponential at

290 K. However, because NO has a much faster (4 orders of magnitude) rebinding time scale than CO, one might reasonably expect that the NO kinetics would be much faster than the protein interconversion time scale, even at room temperature. This should lead to a highly stretched nonexponential response for NO rebinding both above and below  $T_g$ . The fact that this is not observed for NO rebinding points to a fundamental difference between the underlying enthalpic barrier distributions associated with the NO and CO rebinding reactions. Temperature-derivative spectroscopy studies<sup>119</sup> have revealed that the V68 mutations prevent the CO and O<sub>2</sub> movement into the more remote Xe cavities and enhance interactions with the distal histidine. However, if various arrangements of distal pocket amino acid residues and/or ligand-docking site configurations were dominant in determining the enthalpic barrier distributions for CO, then one would expect that NO would be affected in nearly the same way (i.e., the fast phase of the NO rebinding kinetics would show a highly stretched nonexponential decay).

On the other hand, a simple quantitative model for ligand binding to the heme, which focuses on the importance of distributions in the heme geometry,<sup>24</sup> can directly explain both the different time scales and the exponential vs nonexponential behavior associated with the NO and CO rebinding reactions. Figure 9 depicts a cartoon model showing the respective transition states for the NO and CO rebinding reactions for two representative protein/heme conformations. We use the phrase “harpoon model” or “doming model” to describe how we visualize the transition states for the NO and CO rebinding reactions, respectively (see Figure 9). Because NO has an unpaired electron, it is possible to form a transition-state bond with the single electron in the  $d_z^2$  orbital of the high-spin ferrous heme iron atom without first driving the iron into a low-spin configuration. In contrast, the CO molecule has two bonding electrons and the  $d_z^2$  orbital must be depopulated to reach a viable transition state for binding to the heme. We have suggested previously<sup>24</sup> that the enthalpic barrier for such a process can be approximated by  $H_P = (1/2)Ka^2$ , where  $K$  is the force constant associated with heme doming ( $\sim 17$  N/m) and  $a$  is the iron out-of-plane displacement. Thus, what we are suggesting is that the transition state for NO binding can be formed without thermal fluctuations that drive the iron into the heme plane. This concept is consistent with a reactant-like transition state for NO binding, as discussed by Szabo.<sup>120</sup> This is also consistent with recent calculations that show the intermediate spin state of heme NO to be a bound state, in contrast to the situation for heme CO.<sup>117</sup> These calculations provide additional justification for the recombination of NO to an out-of-plane heme iron.

It is noteworthy that the harpoon model is in complete agreement with the observed NO recombination kinetics of cobalt-substituted myoglobin,<sup>38,89</sup> where the cobalt atom does not move out of the heme plane<sup>121</sup> and a NO recombination rate similar to that for the iron-based heme is observed.<sup>38,89</sup> On the other hand, the work presented here indicates that the prior measurements,<sup>86</sup> demonstrating a loss of the second kinetic phase for MbNO at low pH, probably arise primarily from a

(112) Schaad, O.; Zhou, H. X.; Szabo, A.; Eaton, W. A.; Henry, E. R. *Proc. Natl. Acad. Sci. U.S.A.* **1993**, *90*, 9547–9551.

(113) Kholodenko, Y.; Gooding, E. A.; Dou, Y.; Ikeda-Saito, M.; Hochstrasser, R. M. *Biochemistry* **1999**, *38*, 5918–5924.

(114) Ionascu, D.; Gruia, F.; Ye, X.; Yu, A.; Champion, P. M. To be submitted, 2005.

(115) Agmon, N.; Hopfield, J. J. *J. Chem. Phys.* **1983**, *78*, 6947–6959.

(116) Kuczera, K.; Lambry, J. C.; Martin, J. L.; Karplus, M. *Proc. Natl. Acad. Sci. U.S.A.* **1993**, *90*, 5805–5807.

(117) Franzen, S. *Proc. Natl. Acad. Sci. U.S.A.* **2002**, *99*, 16754–16759.

(118) Agmon, N.; Hopfield, J. J. *J. Chem. Phys.* **1983**, *79*, 2042–2053.

(119) Nienhaus, K.; Deng, P. C.; Kriegl, J. M.; Nienhaus, G. U. *Biochemistry* **2003**, *42*, 9647–9658.

(120) Szabo, A. *Proc. Natl. Acad. Sci. U.S.A.* **1978**, *75*, 2108–2111.

(121) Brucker, E. A.; Olson, J. S.; Phillips, G. N.; Dou, Y.; Ikeda-saito, M. J. *Biol. Chem.* **1996**, *271*, 25419–25422.

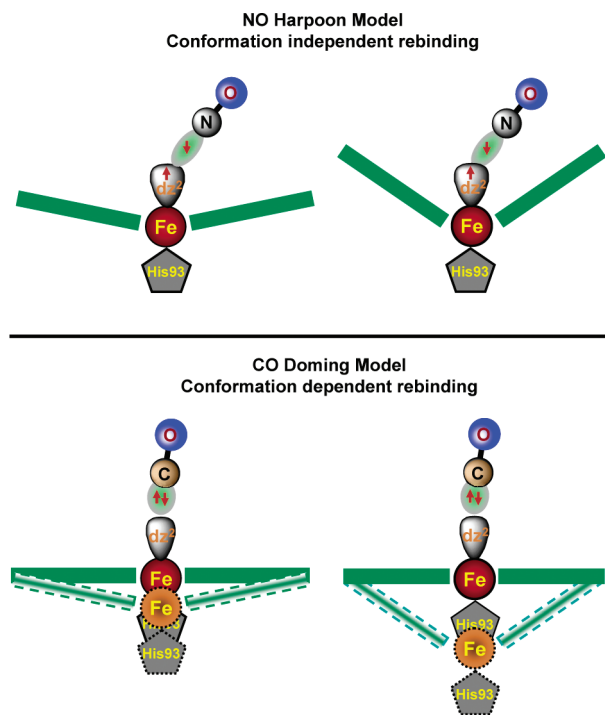


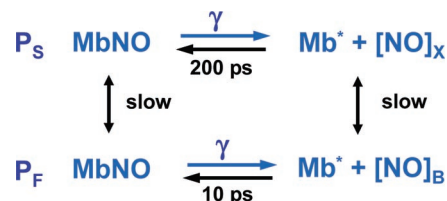
**Figure 9.** Harpoon model for NO binding where the unpaired NO electron and the electron in the  $d_{z^2}$  iron orbital can form a transition state without needing thermal fluctuations to drive the iron into the heme plane. Two different protein/heme conformations are shown and, because the NO “reaches in” and binds to either conformation with the same propensity, the ensemble yields a fast exponential kinetic response. The NO rebinding to iron is fast because the reaction does not need to overcome the heme barrier associated with moving the iron to the in-plane position. In contrast, the CO needs to wait for thermal fluctuations to drive the heme into the planar conformation so that the reaction can occur. As a result, the different initial protein/heme conformations within the ensemble (shown in the lower panels as dashed lines) lead to different enthalpic barriers to reach the common transition state (shown in the lower panels as the planar heme with solid lines). The kinetics in this case will be slower and (when the transition time between the initial conformational substates is slower than the rebinding time scale) nonexponential.

modification of the distal pocket and Xe4 cavity (when the distal histidine is protonated at low pH and swings out toward the solution<sup>90–93,122,123</sup>) rather than from the loss of the proximal histidine.<sup>86</sup>

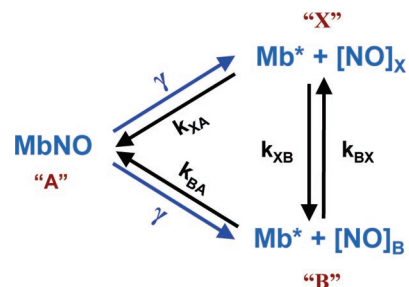
It would obviously be of great interest to test these ideas further by making similar comparisons between cobalt- and iron-based heme in the case of CO binding. Unfortunately, CO does not bind to cobalt heme.<sup>124</sup> However, additional kinetics studies<sup>38</sup> involving  $O_2$  binding to Mb, which should depend to some extent upon the magnitude of heme doming, have shown that the geminate rebinding is much faster ( $\sim 100$  ps) for Co-substituted heme than for the native iron-based heme ( $\sim 30$  ns). This indicates that heme doming remains as an important control mechanism for the regulation of oxygen binding to Mb and Hb.

The harpoon model predicts that the barrier due to the heme iron out-of-plane displacement is effectively absent for the NO reaction. Moreover, because the protein-conformation-induced distribution of iron out-of-plane equilibrium positions is the primary source of the distribution of rebinding barriers for CO

## Scheme 1



## Scheme 2



(at least in the simple linear electron–nuclear coupling version of the doming model<sup>24</sup>), this distribution must effectively collapse for NO binding because the reaction is no longer dependent on the heme geometry distribution. This simple idea explains both the dramatic increase in the NO rebinding rate and the surprisingly homogeneous (i.e., exponential) nature of its time course.

**Kinetic Models.** When NO is used as the kinetic probe molecule, we are better able to discern the underlying details associated with the distal pocket because the distributions due to the proximal heme geometry that dominate the CO rebinding reaction are eliminated. The presence of the two phases in the MbNO kinetics, along with the experiments on the mutant samples (e.g., V68W), has demonstrated that there are at least two separate states associated with the NO ligand in the distal pocket. We denote one of the states as B, in accordance with prior notation, and denote the other state as X, which refers to the likelihood that this state corresponds to the NO in or near the Xe(4) cavity. In the B state, the NO ligand is trapped in the center of the distal pocket, in very close proximity to the heme iron. The state we denote as X may sometimes be referred to as C, or as one of a set of subscripted B states.<sup>49,50,52</sup> However, the two states we invoke in our kinetic analysis are consistent with the recent calculations of Nutt and Meuwly,<sup>67</sup> where the NO is observed near the center of the distal pocket, in close proximity to the iron, as well as in more extended regions in or near the Xe(4) cavity.

Two fundamentally different models that can potentially explain the observed kinetics of MbNO in terms of the B and X states are shown as Scheme 1 and Scheme 2. Scheme 1 uses a coarse-grained kinetic inhomogeneity to explain the two observed phases. The interconversion between two protein conformations is taken to be slow compared to the rebinding reaction rate. Within this model, the fast and slow kinetic phases are associated with the two protein conformations and the populations of the two conformers are allowed to vary to account for the differing amplitudes when the distal pocket is mutated or the glycerol concentration is changed.

The second model (Scheme 2) is kinetically homogeneous and has been previously discussed by Shreve et al.,<sup>96</sup> but with different assignments for the various states (see below). Scheme

(122) Sage, J. T.; Li, P. S.; Champion, P. M. *Biochemistry* **1991**, *30*, 1237–1247.

(123) Quillin, M. L.; Brantley, R. E.; Johnson, K. A.; Olson, J. S.; Phillips, G. N. *FASEB J.* **1992**, *6*, A466.

(124) Hoffman, B. M.; Petering, D. H. *Proc. Natl. Acad. Sci. U.S.A.* **1970**, *67*, 637–643.

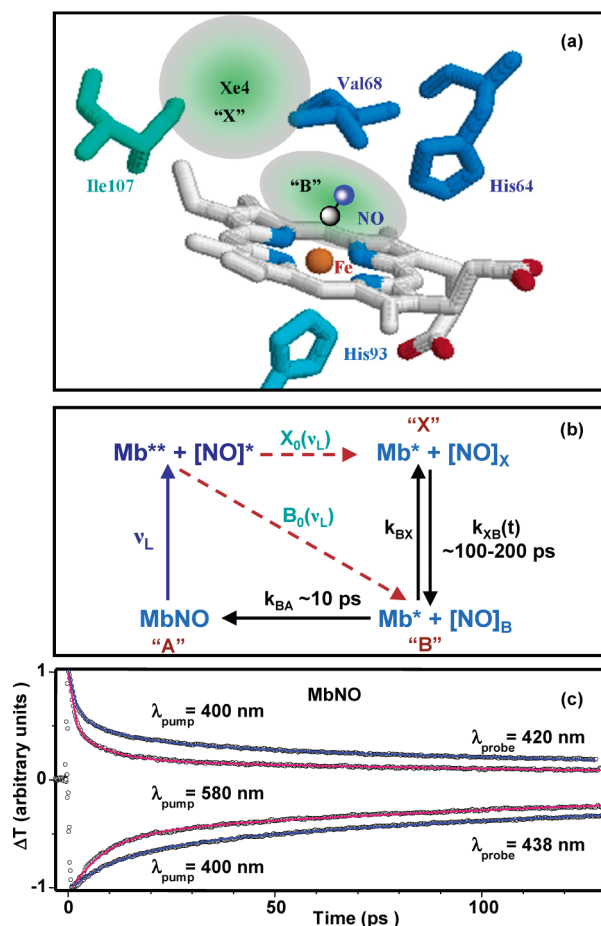


**Figure 10.** (a) Extended distal pocket of the MbNO. (b) Homogeneous NO recombination scheme where the photolyzed NO molecule initially partitions into two subpopulations associated with states B and X. The state Mb\*\* denotes the initial optically excited heme, and the dashed arrows denote the bifurcation of the hot [NO]\* fragment into states B and X. The notation Mb\* denotes the unrelaxed protein following photolysis. (c) Dependence of the NO recombination to Mb upon the pump and probe energy. Note the slow-amplitude decrease as the pump wavelength is increased (decrease in energy) from 400 to 580 nm.

2 invokes a distribution of initial conditions between the B and X states, which is created as the hot photolyzed NO fragment cools and comes to equilibrium. (Here, we have used  $\gamma$  to denote, in the most general sense, the photolysis and redistribution of the ligand in Scheme 2 instead of using explicit state-specific rates  $k_{\gamma X}$  and  $k_{\gamma B}$ .) A more detailed version of the ligand redistribution in Scheme 2 is given in Figure 10b, where we explicitly show the initially excited electronic state of Mb. A distribution of initial conditions ( $B_0$  and  $X_0$ ) is used instead of placing all of the initial population in state B (as is done in the standard three-state serial model). The distribution of the initial population between  $B_0$  and  $X_0$  is necessary to decouple the observed rates and amplitudes, as observed experimentally (i.e., V68 mutation or glycerol concentration changes the relative amplitudes without significantly affecting the rates). This latter issue was stressed by Shreve et al.<sup>96</sup> in their analysis of the glycerol-dependent kinetic amplitudes, and we are in accord with their basic conclusions on this point. However, because the V68 mutant results indicate that state X is associated with the more distant Xe4 site, we consider it unlikely that the NO ligand can make a transition directly from X to the bound state A without first passing through the more localized distal pocket

state B. Thus, we do not believe that the two states represent B state roto-isomers as previously suggested,<sup>96</sup> and to be consistent with an assignment for X in or near the Xe4 pocket, we set  $k_{XA} = 0$  in the final working expressions for the homogeneous model.

To interpret the observed kinetic rates in terms of the fundamental rates shown in Scheme 2, we first express the general solution for the kinetic time course of the individual state populations as

$$B(t) = \frac{1}{\sqrt{D}}[k_{XB}X_0 - B_0(k_{BA} + k_{BX} + K_-)]e^{K_+t} - \frac{1}{\sqrt{D}}[k_{XB}X_0 - B_0(k_{BA} + k_{BX} + K_+)]e^{K_-t} \quad (1a)$$

$$X(t) = \frac{1}{\sqrt{D}}[k_{BX}B_0 - X_0(k_{XA} + k_{XB} + K_-)]e^{K_+t} - \frac{1}{\sqrt{D}}[k_{BX}B_0 - X_0(k_{XA} + k_{XB} + K_+)]e^{K_-t} \quad (1b)$$

Thus, if we use the normalization condition ( $A + B + X = 1$ ), the expression for the observed kinetic time course of the unbound population can be written as

$$1 - A(t) = \frac{1}{\sqrt{D}}[B_0(k_{BA} + K_+) + X_0(k_{XA} + K_+)]e^{K_-t} - \frac{1}{\sqrt{D}}[B_0(k_{BA} + K_-) + X_0(k_{XA} + K_-)]e^{K_+t} \quad (1c)$$

where the other variables in eq 1 are given by

$$D = (k_{BA} + k_{XA} + k_{BX} + k_{XB})^2 - 4(k_{BA}k_{XA} + k_{BA}k_{XB} + k_{XA}k_{BX}) \quad (2a)$$

$$K_{\pm} = \frac{1}{2}[-(k_{BA} + k_{XA} + k_{BX} + k_{XB}) \pm \sqrt{D}] \quad (2b)$$

and the quantities  $X_0$  and  $B_0$  correspond to the initial populations of the X and B states, respectively. The quantities  $K_{\pm}$  are the two observed rates. As can be seen from eq 1c, a Scheme 2 model with an initial condition of  $B_0 = 1$  does not allow for the decoupling of the observed rates from the amplitudes (i.e., the only way to change the amplitudes is to change the rates). On the other hand, when the possibility of a distribution in the initial photolyzed populations between  $X_0$  and  $B_0$  is acknowledged, the amplitudes can be altered by simply changing the initial population distribution.

The mutation studies help us to simplify Scheme 2 and eq 1 because we can set  $k_{XA} = 0$  and, because the fast rate changes only slightly when the transition to and from X is eliminated by the V68W mutation (see Table 1), we can also infer that  $k_{BA} \gg k_{BX}$ ,  $k_{XB}$ . Expansion of the expression for  $\sqrt{D}$  followed by simplification of the rate expressions under the above conditions leads directly to

$$1 - A(t) = I(t) = B_0 e^{-k_{BA}t} + X_0 e^{-k_{XB}t} \quad (3)$$

so that in Scheme 2, with  $k_{BA} \gg k_{BX}$ ,  $k_{XB}$  and  $k_{XA} = 0$ , the experimentally measured rates and amplitudes directly translate to the fundamental rates and initial populations. In the current application for MbNO, the rates of the two observed kinetic

phases differ by at least an order of magnitude (10 and 100 ps) so the  $k_{BA} \gg k_{XB}$  condition is confirmed.

The fact that the observed fast ( $k_{BA}$ ) and slow ( $k_{XB}$ ) rates differ by a factor of 10–20 can also be cross checked independently by considering the following simple approximation. The  $\sim 3$  kJ/mol enthalpic barrier for  $k_{XB}$  accounts for roughly a factor of 6 reduction with respect to  $k_{BA}$  at 200 K (because  $k_{BA}$  has no enthalpic barrier). In addition, the ratio of the ligand accessible volume of the Xe4 pocket to that of the B state distal pocket can be calculated<sup>125</sup> and used to estimate an entropic reduction in the relative transition rates of  $\sim 2.5$  (using equivalent transition-state entropies). This crude approximation yields an overall ratio of  $k_{BA}:k_{XB} \sim 15$ , which is very close to what is observed experimentally.

**Kinetic Selection.** To more clearly differentiate between the inhomogeneous Scheme 1 and the homogeneous Scheme 2, we have performed double pump-pulse kinetic selection experiments<sup>72</sup> on MbNO. The protocol for performing such experiments on ultrafast time scales is significantly different<sup>126</sup> from that used previously for the nanosecond kinetics experiments.<sup>72</sup> However, the basic logic is the same. Namely, for an ensemble of two slowly interconverting conformers with fast and slow ligand-rebinding kinetics, a second delayed pump pulse can be temporally positioned to kinetically select the fast-rebinding subpopulation so that its kinetics can be extracted and compared to the kinetics of the full ensemble (as measured using a single pump pulse). When such experiments are performed, the delay between the two pump pulses can, in principle, be extended until it is longer than the interconversion time between the kinetically distinct conformers so that the kinetics of the selected subpopulation becomes the same as that of the full ensemble. Such experiments were performed on MbNO with delay times between the pump pulses of 10 to 150 ps.<sup>126</sup> In no case did the observed kinetics of the selected subpopulation deviate from that of the full ensemble. Thus, we conclude that the inhomogeneous Scheme 1 can be eliminated as a possible explanation of the MbNO rebinding kinetics.

**Initial Populations.** Within Scheme 2, we find that the hot photolyzed NO fragment must bifurcate between two possible distal sites (B and X) and that the amount of NO that deposits into the X site depends on distal pocket mutations (V68W or V68F), viscosity (glycerol concentration), and the energy of the photon used for photolysis. In Figure 10, we delineate Scheme 2 in more detail, showing the distal pocket architecture (panel a), the kinetics model (panel b), and the result of room-temperature kinetics measurements<sup>15</sup> on MbNO as a function of pump-pulse wavelength (panel c). Because the experimental measurement of the MbNO kinetics effectively reads out the fundamental rates, the observed fast and slow kinetic rate constants correspond to heme rebinding ( $k_{BA}$ ) and the transition from the X site into the B site ( $k_{XB}$ ), respectively. The distribution of initial conditions is found directly from the measured amplitudes so that, from panel c in Figure 10, we see that the relative amplitude of the slow phase is increased when the pump photons become more energetic as the pump wavelength moves to the blue. (The details of the biexponential fits to the more limited time-scale data<sup>15</sup> can be found in Table

**Table 2.** Probe Wavelength-Dependent Rebinding Amplitudes for MbNO

$\lambda_{\text{pump}}$ (nm)	$\lambda_{\text{probe}} = 420$ nm		$\lambda_{\text{probe}} = 438$ nm		$\langle \lambda_{\text{probe}} \rangle$	
	$\tau_i$ (ps)	$A_i$	$\tau_i$ (ps)	$A_i$	$\langle \tau_i \rangle$ (ps)	$\langle A_i \rangle$
400	13.8	0.41	13	-0.35	13.4	0.38
	200	0.59	190	-0.65		
580	8	0.6	8.3	-0.5	8.2	0.55
	170	0.4	170	-0.5		

2; note that the two probe wavelengths in Figure 10c separately follow the bleach and antibleach signals and yield nearly the same results, as expected for a two-electronic-state kinetics process.)

The results shown in Figure 10c are consistent with the idea that a more energetic photon will impart more kinetic energy to the photolyzed NO fragment, making it more probable that the NO finds its way to the more distant distal site X. Because the observed kinetic amplitude for the slow phase directly yields the initial population  $X_0$  (i.e., the amount of photolyzed NO that starts from X), the data indicate that the bifurcation ratio  $X_0:B_0$  is about 1.6 when 400 nm light is used for photolysis and drops to about 0.8 when 580 nm light is used (see Table 2).

**Comparison to CO.** In comparison to NO, the amplitude of CO geminate rebinding is much smaller at room temperature ( $\sim 5\%$ ) so that  $k_{BX} \gg k_{BA}$  and most of the initially hot CO that ends up in or near the Xe4 site (or other X sites) eventually escapes from the protein. The librational and translational disorder associated with the initially photodissociated diatomic molecules might make these transient CO species difficult to detect using either time-resolved infrared or X-ray techniques. However, a significant CO population has been observed<sup>127</sup> in the Xe(4) pocket of the L29F mutant and in the YQR triple mutant,<sup>128</sup> but not in the native protein on picosecond time scales. Unfortunately, the time-resolved X-ray work<sup>127,129</sup> only rarely<sup>130,131</sup> quantifies the absolute CO X-ray scattering intensity, so it is possible that disorder of the dissociated ligand makes it difficult to detect CO in the Xe4 cavity of wt Mb. Moreover, transference of the dynamic information obtained in the time-resolved X-ray studies to the solution phase implicitly assumes that the protein dynamics is independent of the differences between the crystal and solution environments. Early Raman spectroscopic studies that focus on this issue<sup>132,133</sup> suggest that there may be significant differences in the CO escape from crystalline Mb when compared to that of Mb in solution. The significantly retarded approach of MbCO to photostationary equilibrium in the crystalline state, along with the very slow CO rebinding observed in the crystal<sup>132</sup> (cf. Figure 4 of ref 132

(125) Liang, J.; Edelsbrunner, H.; Fu, P.; Sudhakar, P. V.; Subramaniam, S. *Proteins* **1998**, *33*, 18–29.

(126) Yu, A.; et al. To be published, 2005.

(127) Schotte, F.; Lim, M.; Jackson, T. A.; Smirnov, A. V.; Soman, J.; Olson, J. S.; Phillips, G. N., Jr.; Wulff, M.; Anfinrud, P. A. *Science* **2003**, *300*, 1944–1947.

(128) Bourgeois, D.; Vallone, B.; Schotte, F.; Arcovito, A.; Miele, A. E.; Sciarra, G.; Wulff, M.; Anfinrud, P.; Brunori, M. *Proc. Natl. Acad. Sci. U.S.A.* **2003**, *100*, 8704–8709.

(129) Hummer, G.; Schotte, F.; Anfinrud, P. A. *Proc. Natl. Acad. Sci. U.S.A.* **2004**, *101*, 15330–15334.

(130) Srajer, V.; Teng, T. Y.; Ursby, T.; Perman, B.; Bourgeois, D.; Pradervand, C.; Schotte, F.; Kort, R.; Ren, Z.; Royer, W.; Hellingwerf, K.; Wulff, M.; Moffat, K. *Abstr. Pap. Am. Chem. Soc.* **1998**, *216*, 390-HYS.

(131) Srajer, V.; Ren, Z.; Teng, T. Y.; Schmidt, M.; Ursby, T.; Bourgeois, D.; Pradervand, C.; Schildkamp, W.; Wulff, M.; Moffat, K. *Biochemistry* **2001**, *40*, 13802–13815.

(132) Zhu, L. Y.; Sage, J. T.; Champion, P. M. *Biochemistry* **1993**, *32*, 2, 11181–11185.

(133) Zhu, L.; Sage, J. T.; Rigos, A. A.; Morikis, D.; Champion, P. M. *J. Mol. Biol.* **1992**, *224*, 207–215.

and surrounding discussion), suggests that optical pumping may be taking place in the crystal environment, whereas in solution, a more rapid equilibration of CO within the protein matrix is taking place. One must also consider the possibility that NO and CO behave differently as they migrate through the protein. However, it remains possible that the time-resolved X-ray studies of MbCO crystals do actually reflect the spatial and temporal trajectories of NO within solution phase Mb. In that case, the photolyzed CO evidently does not rapidly partition into the Xe4 cavity and state X must then be interpreted as a docking site near this cavity that is somehow blocked or perturbed by the V68 mutations.

We also note that recent work on the kinetics of CO binding to Mb and to a series of PPIX model compounds<sup>102</sup> has found  $H_P$ , the proximal heme barrier (e.g., due to heme doming), to be  $\sim 10$  kJ/mol. In addition to this heme-specific term, the overall barrier for CO rebinding to Mb also includes a roughly equivalent distal pocket barrier,  $H_D \sim 10$  kJ/mol, that is absent in the PPIXCO model systems.<sup>102</sup> Thus, a question arises concerning the absence of the distal barrier in the case of NO rebinding. Although the harpoon model for NO rebinding naturally explains the absence of the proximal heme barrier and the decoupling of the protein conformational substates from the reaction, it does not specifically address the issue of why there is no significant distal rebinding barrier observed for NO.

One possibility is that the distal barrier takes time to develop. Prior work on the geminate rebinding kinetics of MbCO has strongly indicated<sup>69,105</sup> that distal pocket barrier relaxation takes place on nanosecond time scales (following the much faster picosecond heme relaxation). Consistent with this scenario, the NO rebinding to the heme may take place prior to the development of the distal pocket barrier. One potential source of the distal barrier is histidine 64, which may need to be displaced for the CO ligand to bind in its upright position.<sup>134,135</sup> If the relaxation of the distal histidine to a position which blocks the distal binding site takes on the order of nanoseconds or longer, this would be consistent with the various kinetic observations. Alternatively, the bent nature of the Fe–NO ligand geometry (in contrast to the linear Fe–CO geometry) would also be a simple way to explain the lack of the distal rebinding barrier for NO (i.e., with the bent conformation, it may not be necessary to displace the distal histidine 64 residue<sup>97,136</sup>).

**Barrier Relaxation for  $k_{XB}$ .** Finally, we would like to draw attention to the fact that, in Figure 10b, we have indicated that the transition from state X to state B appears to involve a process with a time-dependent free-energy barrier; i.e., the rate  $k_{XB}(t)$  is shown explicitly to have time dependence. We suggest this because of the distinctly “stretched” character of the slow-phase kinetics in MbNO, which corresponds to the transition from X to B. In addition, we have considered the recent state-specific kinetics of the MbNO reaction intermediates obtained using time-resolved infrared techniques.<sup>52,137</sup> Our analysis suggests that a kinetics scheme such as that outlined in Figure 10b offers a self-consistent explanation for both the vibrationally specific (IR)<sup>52</sup> and the electronically specific (optical) measurements presented here.

We note that Scheme 2 (Figure 10b) differs from the recent model proposed on the basis of IR kinetics measurements alone.<sup>52</sup> The four-state IR model<sup>52</sup> (A, B<sub>0</sub>, B<sub>1</sub>, B<sub>2</sub>) invokes a time-dependent rate and relaxation in the B  $\rightarrow$  A transition that is not observed in the (exponential) fast geminate phase data presented here. However, the IR model can be made equivalent to the three-state model (A, B, X) presented in Scheme 2, if the  $\sim 2\%$  IR minority state, B<sub>2</sub>, is neglected and the rebinding to A is taken to proceed through B<sub>0</sub> rather than B<sub>1</sub> (i.e., B<sub>0</sub> and B<sub>1</sub> in ref 52 become, respectively, B and X in Scheme 2). The mutant studies and double pump-pulse kinetics reported here solidify these assignments. Moreover, a simulation of the measured IR population decays indicates that Scheme 2 (Figure 10b) yields an equivalent fit to the IR data when compared to the fit using the model<sup>52</sup> suggested by the IR data alone.

## Conclusion

This work presents the first comprehensive measurements of the temperature-dependent NO rebinding kinetics of Mb and its distal pocket mutants. Rebinding of NO to protoporphyrin IX in glycerol is also studied so that the effect of the surrounding protein material can be assessed. We conclude that the two kinetic phases observed in Mb correspond to fast rebinding of NO from a localized state (B) near the heme ( $k_{BA} \sim 10$  ps) and a slower (time-dependent) transition ( $\langle k_{XB}(t) \rangle \sim 200$  ps) that monitors the motion of the ligand from a somewhat more distant site (e.g., in or near the Xe4 pocket) to the localized B state. The fast transition for NO has no enthalpic barrier and shows no evidence for the existence of a broad distribution of protein conformational substates, in stark contrast to what is observed for CO binding to Mb at low temperature. This observation can be easily explained if the transition state for NO binding is reactant-like and the extra unpaired electron on the NO molecule “harpoons” the heme iron atom without it having to be driven into the heme plane by thermal fluctuations. Moreover, the exponential nature of the dominant (10 ps) NO rebinding process shows that the NO reaction is decoupled from the protein conformational substates. This strongly implies that the non-exponential kinetics observed for CO rebinding at low temperatures<sup>18</sup> arises primarily from the quenched distribution of heme iron out-of-plane displacements.<sup>24</sup> The temperature-dependent kinetics also reveals that the slow transition has a small enthalpic barrier ( $\sim 3$  kJ/mol), which is self-consistent with the relative time constants of the two kinetic phases when the respective volumes of the distal pocket and the Xe4 cavity are considered. Finally, for MbNO, the relative amplitudes of the fast and slow kinetic responses depend on distal mutation, viscosity, and the photon excitation wavelength. In contrast to the mutation and viscosity perturbations, which suppress the slow phase, more photon energy in the photolysis step leads to an increased probability that the NO ligand will find its way to a more distant site, X (in or near the Xe4 cavity).

**Acknowledgment.** This work was supported by NIH (DK035090) and NSF (DMB 0211816) to P.M.C. and by NIH grants GM 35649 and HL 47020 to J.S.O. J.S.O. is also supported by the Robert A. Welch Foundation grant C-0612.

JA054249Y

(134) Lim, M.; Jackson, T. A.; Anfirud, P. A. *Science* **1995**, *269*, 962–966.

(135) Sage, J. T. *J. Biol. Inorg. Chem.* **1997**, *2*, 537–543.

(136) Miller, L. M.; Pedraza, A. J.; Chance, M. R. *Biochemistry* **1997**, *36*, 12199–12207.

(137) Kim, S.; Jin, G.; Lim, M. *J. Phys. Chem. B* **2004**, *108*, 20366–20375.